

1 **The influence of multiple groups of biological ice nucleating particles on microphysical**
2 **properties of mixed-phase clouds observed during MC3E**

3

4

5 Sachin Patade^{1*}, Deepak Waman¹, Akash Deshmukh¹, Ashok Kumar Gupta², Arti Jadav¹,

6 Vaughan T. J. Phillips¹, Aaron Bansemer⁴, Jacob Carlin³, Alexander Ryzhkov³,

7

8 ¹Department of Physical Geography and Ecosystem Science, Lund University, Lund, Sweden

9 ²Department of Earth and Environmental Sciences, Vanderbilt University, Nashville, TN,
10 37240, USA

11 ³Cooperative Institute for Severe and High-Impact Weather Research and Operations, The
12 University of Oklahoma, and NOAA/OAR National Severe Storms Laboratory, Norman,
13 Oklahoma, USA

14 ⁴National Center for Atmospheric Research, Boulder, Colorado, USA

15

16

17

18

19

20

21

22

23

24 *** Corresponding Author**

25 **Dr. Sachin Patade, Lund University, Sweden**

26 **email: sachin.patade@nateko.lu.se**

27

28

29

30

Abstract:

A new empirical parameterization (EP) for multiple groups of primary biological aerosol particles (PBAPs) is implemented in the aerosol-cloud model (AC) to investigate their roles as ice-nucleating particles (INPs). The EP describes the heterogeneous ice nucleation by (1) fungal spores, (2) bacteria, (3) pollen, (4) detritus of plants, animals, and viruses, and (5) algae. Each group includes fragments from the originally emitted particles. A high-resolution simulation of a midlatitude mesoscale squall line by AC is validated against airborne and ground observations.

Deleted: ¶

Sensitivity tests are carried out by varying the initial vertical profiles of the loadings of individual PBAP groups. The resulting changes in warm and ice cloud microphysical parameters are investigated. The changes in warm microphysical parameters including liquid water content, and cloud droplet number concentration are minimal ($< 10\%$). Overall, PBAPs have little effect on ice number concentration ($< 6\%$) in the convective region. In the stratiform region, increasing the initial PBAP loadings by a factor of 1000 resulted in less than 40% change in ice number concentrations. The total ice concentration is mostly controlled by various mechanisms of secondary ice production (SIP). However, when SIP is intentionally shut down in sensitivity tests, increasing the PBAP loading by a factor of 100 has less than a 3% effect on the ice phase. Further sensitivity tests revealed that PBAPs have little effect on surface precipitation as well as on shortwave and longwave flux ($< 4\%$) for 100-fold perturbation in PBAPs.

Formatted: Indent: First line: 1,27 cm

1. Introduction

In most climate models, the largest source of uncertainty for estimating the total anthropogenic forcing is associated with cloud-aerosol interactions (Pörtner et al., 2022). Atmospheric aerosol particles can act as cloud condensation nuclei (CCN) and a few of them

Deleted: ¶

59 act as ice-nucleating particles (INPs), thereby influencing the microphysical properties of
60 clouds and, depending on the cloud type (Fan et al. 2010; Chen et al 2019). The treatment of
61 INP in climate models can strongly affect the atmospheric radiation budget (DeMott et al.
62 2010). Various sources of aerosol particles, including dust/metallic, marine aerosols,
63 anthropogenic carbonaceous emissions, and primary biological aerosol particles (PBAPs),
64 contribute to the observed INPs (Kanji et al. 2017).

Deleted: ¶

65 A significant amount of global precipitation is associated with the ice phase in cold
66 clouds (Heymsfield and Field 2015; Mülmenstädt et al. 2015, Heymsfield et al. 2020). In
67 particular, mixed-phase clouds are vital for the global climate (Dong and Mace 2003;
68 Zuidema et al. 2005; Matus and L'Ecuyer 2017; Korolev et al. 2017 and references therein).
69 In a multimodel simulation study, Tsushima et al. (2006) showed that the doubling of CO₂
70 concentrations caused the changes in the distribution of cloud-water in the mixed-phase
71 clouds in a climate simulation to be significant.

Formatted: Indent: First line: 1,27 cm

Deleted: ¶

72 PBAPs are solid particles of biological origin and are emitted from the Earth's surface
73 (Després et al. 2012). They are highly active in initiating ice as INPs and include bacteria,
74 fungal spores, pollen, algae, lichens, archaea, viruses, and biological fragments (e.g., leaf
75 litters, insects) and molecules (e.g., proteins, polysaccharides, lipids) (Després et al., 2012;
76 Fröhlich-Nowoisky et al., 2015; Knopf et al., 2011; Szyrmer and Zawadzki, 1997;).
77 Considering the onset temperature of freezing, some ice nucleation active fungi and bacteria
78 (especially *Pseudomonas syringae* with onset freezing temperature around -3°C) are among
79 the most active INPs present in the atmosphere (Després et al. 2012; Hoose and Möhler
80 2012). The potential impact of PBAP INPs on cloud microphysical characteristics has been
81 recognized for many years; however, this topic remains a subject of debate (DeMott and
82 Prenni 2010; Spracklen and Herald, 2014; Hoose et al. 2010b). Some previous modeling
83 studies have shown that on a global scale PBAPs have only a limited influence on clouds and

precipitation (Hoose et al. 2010; Sesartic et al. 2012, 2013; Spracklen and Heald 2014). On a global scale, the percentage contribution of PBAPs to the immersion freezing (ice nucleation by INP immersed in supercooled water drop) is predicted to be much smaller (0.6%) as compared to dust (87%) and soot (12%) (Hoose et al. 2010).

Deleted: ¶

Many studies have used cloud models to highlight the potential impact of PBAP INPs on cloud microphysics and precipitation (e.g., Levin et al. 1987; Grützun et al. 2008; Phillips et al. 2009). For example, the mesoscale aerosol-cloud model by Phillips et al. (2009) had a 3-D domain of about 100 km in width, and many cloud types were present in the mesoscale convective system that was simulated. Their simulations revealed that the cloud cover, domain radiative fluxes, and surface precipitation rate were significantly altered by boosting organic aerosols representing PBAPs. According to Hummel et al. (2018) in shallow mixed-phase clouds (i.e., altostratus) when the cloud top temperature is below -15°C, PBAPs have the potential to influence the cloud ice phase and produce ice crystals in the absence of other INPs.

Deleted: ¶

The quest for insights into the broader atmospheric role of PBAP INPs for cloud microphysical properties and precipitation is hampered by the limited availability of observations both of their ice nucleation activities for various species and their aerosol distributions in the real atmosphere (Huang et al. 2021). More generally, there is incomplete knowledge about the chemical identity of the key INPs, whether biological or otherwise (Murray et al. 2012). In many global and regional models, the ice nucleation activity of bioaerosols is represented either empirically or theoretically based on laboratory measurements of specific biological species of PBAPs that are assumed as representative candidates (e.g., *Pseudomonas syringae*). This assumption of representativeness introduces uncertainties that would be expected to impact the model results, potentially introducing a

112 bias into the estimation of the effects of bioaerosols on clouds (e.g. Sahyoun et al., 2016;
113 Hoose et al. 2010b; Spracklen and Herald, 2014, Huang et al. 2021 and references therein).

114 In addition to primary ice nucleation, ice formation in clouds can occur because of
115 processes generating new particles from pre-existing ice, and these are known as Secondary
116 Ice Production (SIP) mechanisms (Korolev and Leisner, 2020; Korolev et al, 2020). SIP can
117 have a considerable impact on cloud micro- and macro-physical properties such as
118 precipitation rate, glaciation time, cloud lifetime, and cloud electrification by increasing the
119 ice number concentrations by a few orders of magnitude (e.g., Blyth and Latham 1993;
120 Crawford et al., 2012; Lawson et al., 2015; Phillips et al., 2017b, 2018, 2020; Phillips and
121 Patade, 2021; Sotiropoulou et al. 2021a,b). This in turn can influence the global hydrological
122 cycle and climate (Zhao and Liu 2021).

123 However, in many cloud models, the representations of these SIP mechanisms are
124 uncertain as most of the cloud models include only the Hallet-Mossop (hereafter HM; Hallett
125 and Mossop, 1974) process and neglect other SIP mechanisms (e.g. Fan et 2017; Han et al
126 2019). A few secondary ice formation processes (e.g., the HM process) have been suggested
127 to be active in the temperature range where active PBAP INPs exhibit strong ice nucleation
128 activity. The INPs of biological origin such as bacteria are highly active in the temperature
129 range of the HM process (-3 to -8°C) as compared with non-biological INPs (Möhler et al.
130 2008; Patade et al., 2021, henceforth PT21). At temperatures warmer than -15°C, some of the
131 PBAPs generated by biologically active landscapes (e.g. forests, woodlands) can promote ice
132 formation and crystal growth in clouds (Morris et al., 2014).

133 In the USA, about 18% of the total landmass is used as cropland, farmland, and
134 agricultural activities (Garcia et al. 2012). These are major sources of biological particles in
135 the atmosphere. Biogenic particles released from crops, either pre- and post-harvest, have

Deleted: ¶

Deleted: . For example,

Deleted: (

Deleted: demonstrated using a global climate model that SIP dominates ice formation in moderately cold clouds and has a significant influence on their liquid and ice water paths. They showed that including three SIP mechanisms in the model simulated global annual average liquid water path decreases by 15 g m^{-2} (-22% change) and the ice water path increases by 9 g m^{-2} (23%), resulting in better agreement with observations. Accounting for SIP in their model results in a change in the global annual average net cloud radiative forcing by about 1 W m^{-2} . Although a small fraction of the total cloud radiative forcing globally, this flux change underlines the ubiquitous role of SIP on cloud properties on the large scale.¶

Deleted: ¶

153 previously been shown to serve as INPs (in Colorado and Nebraska, Garcia et al. 2012).
154 Huffman et al. (2013) found that airborne biological particles increase significantly in
155 concentration, by an order of magnitude or more, during rainfall in a forest in the western US
156 and that bioaerosols are well correlated with INPs. Prenni et al. (2013) observed a similar
157 increase in concentrations of ground-level INPs during rain at a forested site in Colorado,
158 which was associated with increased biological particles. Convective clouds can efficiently
159 transport lower tropospheric aerosol particles into the upper troposphere where they can
160 affect the cloud properties (Cui and Carslaw, 2006)

Deleted: If these potential INPs are detrained from the convective outflow of a cell at mid-levels, then they may be entrained into other clouds aloft, influencing the microphysical properties of that subsequent storm. ...

161 The current study aims to simulate realistic concentrations of multiple groups of
162 PBAP INPs, including bacterial and fungal particles, to investigate their interactions with
163 convective clouds observed during the Midlatitude Continental Convective Clouds
164 Experiment field campaign (MC3E), in the USA (Jensen et al. 2016), in the USA. In view of
165 the literature noted above about the effects of PBAP INPs, there is a need for more detailed
166 analyses of their role in altering cloud microphysical properties and precipitation because the
167 realistic treatment of ice nucleation activity for major PBAP groups was not available, prior
168 to our empirical scheme (PT21). Hitherto, laboratory measurements of isolated biological
169 species (e.g., *Pseudomonas syringae*, *Cladosporium sp*) have been the basis for attempts to
170 simulate biological ice nucleation in clouds, but the representativeness of the choice of such
171 species has been a longstanding issue. For example, Hummel et al (2018) considered three
172 highly ice-nucleation-active PBAP species in their model which may not represent the ice
173 nucleation activity of PBAP in the atmosphere. It is not known which biological species of
174 ice nucleation active (INA) PBAPs contribute the most to biological ice nucleation.
175 Consequently, there is a need for a new approach oriented toward laboratory measurements
176 of biological INPs sampled from the atmosphere, thus optimizing the representativeness of
177 the data for studies of clouds.

Deleted: ¶

In this paper, such an approach is followed to investigate the effect on cloud properties from various major groups of PBAP. We incorporated a recent empirical parameterization for various PBAP groups by PT21 into our 3D aerosol-cloud model (AC). PT21 created an empirical formulation resolving the ice nucleation of each group of PBAPs including 1) fungal spores and their fragments, 2) bacteria and their fragments, 3) pollen and their fragments, 4) detritus of plants, animals, and viruses, and 5) algae. We also examine the relative importance of various secondary ice processes in their role in mediating the PBAP effects on cloud microphysical properties, given the weakness of PBAP effects on cloud microphysical properties.

2. Description of observations

2.1 Selected case of a deep convective system

In the current study, we simulated a squall line that occurred on 20 May 2011 MC3E (Jensen et al. 2016). The MC3E campaign took place from 22 April through to 6 June 2011 and was centered at the Atmospheric Radiation Measurement (ARM) Southern Great Plains (SGP) Central Facility (CF), (36.6°N, 97.5°W) in north-central Oklahoma. The surface meteorological analysis on 20 May indicated a southerly flow at the surface, which provided enough moisture from the Gulf of Mexico to trigger convection. Deep convection, organized in the form of a squall line, passed over the measurement site between 1030 and 1100 UTC, resulting in convective precipitation. It was followed by widespread stratiform precipitation that was well observed by both airborne and ground-based measurements. Vertical sounding characteristics of this case are described in Supplement Information (Figure S1) based on Skew-T plot.

Deleted: ¶

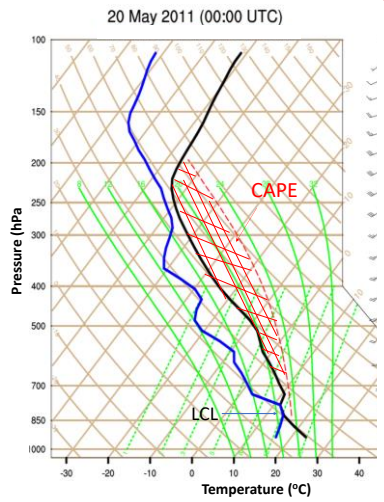
Deleted: The empirical formulation by PT21 is based on observations of PBAP collected at the Amazon Tall Tower Observatory (ATTO). It is a research site located in the middle of the Amazon rainforest in northern Brazil. In this article, wW

Deleted: ¶

Deleted: Jensen et al. (2016) describe the squall line as a "golden event" of the MC3E campaign given the robust *in situ* sampling of extensive stratiform outflow from deep convection on this day. ...

Deleted: ¶

The skew-T plot from the radiosonde sounding conducted on 20 May 2011, at (00 UTC) is shown in Figure 1a. The skew-T plot shows the vertical sounding before the formation of deep convection. The skew-T plot shows that the surface-based Convective Available Potential Energy (CAPE) for this case was 2400 J kg^{-1} , and the Lifting Condensation Level (LCL) was located at 840 hPa. The temperature at LCL, which is generally at the same height as the convective cloud base, was 15°C . The vertical profile of the water vapor mixing ratio is also shown in Figure 1b. The water vapor mixing ratio at the surface was around 11.8 g kg^{-1} which decrease rapidly to 2 g kg^{-1} at 5 km. ¶



Deleted:

Figure 1. (a) The skew T plot from May 20, 2011, sounding. The air temperature is represented by the solid black line, while the dew point temperature is represented by a dashed grey line. The moist adiabats is represented by a dotted red line. The shaded region between moist adiabats and temperature line represents convective available potential energy (CAPE). The LCL is also mentioned in the plot. (b) Vertical profile of water vapor mixing ratio on 20 May 2011 at 00 UTC. ... ¶

¶

243 2.2 Aircraft Observations

244 The in-situ cloud microphysical observations used in this study were obtained from a

245 University of North Dakota Citation II aircraft. The aircraft collected observations of cloud

246 microphysical parameters from the cloud base (1.8 km above mean sea level; hereafter MSL)

247 to a maximum altitude of 7.5 kilometers above MSL. The MC3E campaign collected

248 extensive airborne measurements of aerosols and cloud microphysical properties over north-

249 central Oklahoma. A detailed description of the scientific objectives of the MC3E program,

250 including the field experiment strategy, airborne and ground-based instrumentation, is given

251 in the paper by Jensen et al. (2016). A summary of the airborne instrumentation during

252 MC3E is provided in Supplementary Information.

Deleted: ¶

Deleted: *in situ*

Deleted: This section summar

Deleted: izes

Deleted: the

Deleted: used in the current study

Deleted: Table 1: Details of aircraft instruments used in this study.¶

Instrument

255 2.3 Ground-based measurements

256 A comprehensive instrumentation suite deployed at the ARM-SGP central facility provided

257 continuous measurements of atmospheric gases, aerosols, clouds, and local meteorological

258 conditions (e.g., wind, temperature, precipitation, and atmospheric profiles). A cloud

259 condensation nuclei (CCN) counter (CCN-100) (DMT) measured the CCN number

260 concentration at seven supersaturation values with a temporal resolution of 1 hour. Surface

261 precipitation was measured with 16 rain gauge pairs placed within a 6-kilometer radius of the

262 SGP CF.

263 During the MC3E campaign, the measurement facility deployed at CF measured the

264 spatial variability of surface fluxes of heat, moisture, and momentum. A radiosonde array of

265 6 sites, covering an area of 300 km × 300 km, was designed to capture the large-scale

266 variability of the atmospheric state. Radiosonde observations (Vaisala RS92-SGP) were

267 conducted with a 6-hour frequency (four times daily) at around 05:30, 11:30, 16:30, and

Deleted: ¶

279 22:30 UTC, providing vertical profiles of atmospheric state variables (pressure, temperature,
280 humidity, and winds) of the environment surrounding the ARM SGP site. When aircraft
281 operations were planned based on forecasted convective conditions, the sounding frequency
282 was increased to a 3-hour frequency with the starting time at 05:30 UTC.

283 In addition to airborne observations, the ARM radar network was used to conduct
284 unique radar observations during the MC3E campaign. The information about various radar
285 assets during MC3E is given by Jensen et al. (2016). The surface precipitation used for model
286 validation in this study is a radar-based precipitation estimate as described by Giangrande et
287 al. (2014). Their radar-based rainfall retrievals were in good agreement with observations
288 with an absolute bias of less than 0.5 mm for accumulations less than 20 mm.

289 The Interagency Monitoring of Protected Visual Environments (IMPROVE) network
290 stations close to the location of airborne observations provided ground-level measurements of
291 various chemical species. These included carbonaceous compounds (black and organic
292 carbon), salt, ammonium sulfate, and dust. The details of the measurement techniques used
293 for mass mixing ratios of these compounds are summarized in Malm et al. (1994). The
294 measurements of these aerosol species from various IMPROVE sites, including Ellis
295 (36.08°N, 99.93°W), Stilwell (35.75°N, 94.66°W), and Wichita Mountains (34.73 °N,
296 98.71°W) sites in Oklahoma, were averaged to provide inputs to AC.

297 Initial mass concentrations for the aerosol species of AC (11 species) including
298 sulfate, sea salt, dust, black carbon, soluble organic, biological and non-biological insoluble
299 organic (five groups of PBAPs) were derived from the Goddard Chemistry Aerosol Radiation
300 and Transport (GOCART) model (Chin et al. 2000). The prescribed mass mixing ratios of
301 aerosol species in A are based on IMPROVE observations and are enlisted in [Supplementary](#)
302 [Information](#) (Table S2). It should be noted that for the MC3E case considered in this study,

Deleted: ¶

Deleted: They used radar observations from the C-band and X-band scanning ARM precipitation radars (C-band Scanning ARM Precipitation Radar and X-band Scanning ARM Precipitation Radars, respectively) to estimate rainfall within 100 km of the ARM facility in Lamont, Oklahoma. Their

Deleted: ¶

Formatted: Indent: First line: 1,27 cm

Formatted: Not Highlight

310 coincident IMPROVE measurements were not available. The mean values of the IMPROVE
311 measurements conducted on May 18 and 21 are used to prescribe the mass of various aerosol
312 species.

314

315 **3. Methodology**

316 *3.1 Model description*

317 The ‘aerosol-cloud model’ (AC) used in this study is a cloud-resolving model (CRM) with a
318 hybrid spectral bin/two-moment bulk microphysics, interactive radiation, and semi-
319 prognostic aerosol schemes (Phillips et al. [2017b](#), 2020). The model predicts the mass and
320 number concentrations for five types of hydrometeors: cloud liquid, cloud ice (or “crystals”),
321 rain, graupel/hail, and snow. The mixing ratios of the total number and mass of all particles in
322 each microphysical species are treated as model prognostic variables. AC treats all known
323 microphysical processes such as droplet nucleation, ice initiation through primary and
324 secondary processes, and growth processes such as deposition/sublimation of ice particles,
325 condensation/evaporation of drops, freezing/melting, as well as coagulation by collisions
326 between various hydrometeor types. Both cloud-base and in-cloud activation of aerosols to
327 form cloud-droplets are treated explicitly, with the predicted in-cloud supersaturation
328 resolved on the model grid being used to activate aerosols aloft. Bin-resolved size
329 distributions of each aerosol species are predicted for the interstitial and immersed
330 components of each aerosol species. Extra prognostic variables track the number of aerosols
331 in each aerosol species that have been lost by INP and CCN activation.

332 Secondary ice formation is represented by four types of fragmentation:

- 333 • breakup in ice–ice collisions (Phillips et al. 2017a, b) (most active between -10 to -
334 20°C);

Deleted: Table 2: The mass mixing ratio of aerosol species based IMPROVE observations which are used as input to AC.¶
Aerosol species

Deleted: ¶

Deleted: 2017a

Deleted: ¶

- Hallett and Mossop (1974), rime splintering (most active between -3 to -8°C);
- fragmentation of freezing rain/drizzle by modes 1 and 2 (Phillips et al. 2018) (most active around -15°C);
- and sublimation breakup (Deshmukh et al. 2021) (most active between -0 to -18°C).

Deleted:

The empirical parameterization (EP) (Phillips et al. 2013) of heterogeneous ice nucleation treats all known modes of ice formation (deposition mode, condensation-/immersion-freezing, inside-out and outside-in contact-freezing) in terms of dependencies on the loading, size, and chemistry of multiple aerosol species. In the previous version of the EP, prior to PT21, there were four species of INP aerosol. One of these was PBAP INPs. However, that version of the EP did not resolve the individual types of PBAP INP, which exhibit a wide range of ice-nucleating abilities. The current version of AC also includes the ice nucleation (IN) activity of dust and black carbon. The ice nucleation parameterization of dust, as well as black carbon, is based on studies by Phillips et al. (2008) and (2013). The activation of dust and black carbon INP starts at temperatures colder than -10 and -15°C.

There are two types of homogeneous freezing represented: that of cloud droplets near -36°C and that of solute aerosols at colder temperatures. Both schemes are described by Phillips et al. (2007, 2009). For cloud droplets, a look-up table from simulations with a spectral bin microphysics parcel model treats the fraction of all supercooled cloud droplets that evaporate without freezing near -36°C, depending on the ascent, initial droplet concentration, and supersaturation. The size dependence of the temperature of homogeneous freezing is represented.

Deleted: ¶

Cloud processes and rainfall formation have been detected using different radar variables, such as specific differential phase K_{DP} . Moisseev et al. (2015), for example, noted an increase in observed K_{DP} because of aggregation. In addition, a few studies have

Deleted: ¶

In a recent study, PT21 provided an empirical formulation for multiple groups of PBAP INPs based on field observations over the central Amazon. In this study, we modified AC by implementing the recent empirical parameterization of PBAP INPs by PT21. A summary of their formulation is provided in section 3.2. ¶

hypothesized evidence of SIP via K_{DP} (e.g., Sinclair et al. 2016; Kumjian and Lombardo 2017; Carlin et al. 2021). In this study, we attempted to detect secondary ice formation signatures by implementing K_{DP} estimations into AC. Based on Ryzhkov et al. (2011), K_{DP} values were estimated for various hydrometeor types, including cloud drops, raindrops, cloud ice, snow, and graupel (their equations 22, 23, 24, 26, and 29).

3.2 Empirical formulation for PBAP INPs:

In a recent study, PT21 provided an empirical formulation for multiple groups of PBAP INPs based on field observations over the central Amazon. In this study, we modified AC by implementing the recent empirical parameterization of PBAP INPs by PT21. The empirical formulation by PT21 is based on observations of PBAP collected at the Amazon Tall Tower Observatory (ATTO), a research site located in the middle of the Amazon rainforest in northern Brazil. The empirical formulation by PT21 for multiple groups of PBAPs includes: - 1) fungal spores (FNG), 2) bacteria (BCT), 3) pollen (PLN), 4) viral particles, plant/animal detritus (DTS), 5) algae (ALG) and their respective fragments are implemented in AC. This formulation has empirically derived dependencies on the surface area of each group (except algae) and it applies to particles with diameters greater than 0.1 μm . Additional details about the formulation by PT21 are given in Supplementary Information.

3.3 Model setup

AC was driven by initial and evolving boundary data for meteorological conditions. The large-scale advection of humidity and temperature tendencies maintained the convection.

Deleted: The scattering amplitudes were calculated using the Rayleigh approximation. The K_{DP} estimations are made for 0° elevation angle and S-band (radar wavelength of 11 cm). The equivalent volume diameter of the given hydrometeor was used for all calculations.

Deleted: ¶

Deleted: is based primarily on field observations over the central Amazon rainforest, withhas

Deleted: the

Deleted: Here, we summarize

Deleted: briefly

Deleted: .

Formatted: Indent: First line: 1,27 cm, Space Before: 0 pt

Deleted: For $X = \text{FNG, PLN, BCT, and DTS}$ ¶

$$n_{IN,BIO,X} = \int_{\log[0.1 \mu\text{m}]}^{\infty} \{1 - \exp[-\mu_X]\} \times \frac{dn_X}{d\log D_X} d\log D_X, \quad (1) ¶$$

$$\mu_X = H_X(S_i, T) \xi(T) \times \text{MIN}\{\exp(-\gamma_X T) - 1, 40\} \times \frac{1}{\omega_{X,1*}} \frac{d\Omega_X}{dn_X} \quad \text{for } T < 0^\circ\text{C} \quad (2) ¶$$

In equation (1), $n_{IN,BIO,X}$ is the number mixing ratio of INP active at temperature T for given species X ; Ω_X is the total surface area mixing ratio of particles with diameters D_X greater than 0.1 μm ; $d\Omega_X/dn_X \approx \pi D_X^2$. The normalized size distribution of given bioaerosol species is given by $dn_X/d\log D_X$. In Eq (2), H_X is the empirically determined fraction that inhibits nucleation in substantially water-saturated conditions. The factor ξ varies between 0 to 1 and considers the fact during laboratory experiments drop freezing was not observed at temperatures warmer than a certain threshold in the laboratory observations. The parameter $\omega_{X,1*}$ depends on bioaerosol type with the dimensions of area (m^2). The values of $\omega_{X,1*}$, shown for PLN and DTS are 0.1 m^2 . For FNG and BCT the values of $\omega_{X,1*}$ are 9.817×10^{-5} and $9.12 \times 10^{-5} \text{ m}^2$ respectively. The slope of the fitted curve (γ_X) has a constant value of 0.5 C^{-1} . ¶

The concentration of algal particles at the ATTO site was much smaller than our detection threshold, so we could not use a similar empirical treatment for ALG. The frozen fraction for the algal particles (Diatom cell, *Thalassiosira pseudonana*) available in the literature is used to estimate INPs from ALG (Wilson et al. 2015). The frozen fraction is given by eq. (3) ¶

$$f_{algae}(T) = A_1 + \frac{(A_2 - A_1)}{1 + 10^{(B+T) \times p}} \quad (3) ¶$$

where $A_1 = -0.03$, $A_2 = 0.993$, $B = 27.73$, and $p = 0.399$. Also $f_{algae}(T) = 0$ at $T > -24^\circ\text{C}$ and $f_{algae}(T) = 1$ at $T < -35^\circ\text{C}$ ¶

For the given concentration of algal particles in the air (n_{algae}) the active INP from ALG is given by ¶

$$n_{IN,BIO,X} = f_{algae} \times n_{algae} \quad (4) ¶$$

¶
¶

448 Convection was initiated by imposing perturbations onto the initial field of vapour mixing
 449 ratio. The large-scale forcing condition used for the simulation was derived using the
 450 constrained variational analysis method described in Xie et al (2014). Based on this method,
 451 the so-called large-scale forcing including large-scale vertical velocity and advective
 452 tendencies of temperature and moisture were derived from the sounding measurements
 453 network. During the MC3E campaign, the sounding network consists of five sounding
 454 stations centered on a sixth site at the ARM SGP central facility. An area with a diameter of
 455 approximately 300 km was covered by this sounding network covers. The supplementary
 456 Figure S2 shows the time height evolution of potential temperature and water vapor mixing
 457 ratio from large-scale forcing data. It also shows the time variation of CAPE based on
 458 observations. The maximum value of CAPE 2400 JKg^{-1} was noticed around 12 UTC on 20th
 459 May.

Deleted: (CF)

Deleted: Additional details about the sounding data are described in section 2.3. ...

Deleted: S1

Deleted: ¶

460 The model simulations were carried out for a three-dimension domain of 80 km x 80
 461 km with horizontal grid spacings of 2 km. In vertical, the model resolution was 0.5 km, and
 462 the model top was located at about 16 km. The lateral boundary conditions are doubly
 463 periodic on all sides of the domain. The initial time of the simulations was at 1200 UTC on
 464 19 May 2011 and all simulations were performed for 48 hours at a time step of 10 seconds.

Deleted: ¶

465 The GOCART model (Chin et al. 2000) was used to initialize the seven chemical
 466 species associated with the EP. The data from the three IMPROVE sites mentioned above
 467 (Section 2.3) was used to rescale the mass concentration profiles at all levels so that they
 468 match the measurements near the surface. Table S2 in Supplementary Information lists the
 469 mass mixing ratios of various aerosol species after the corrections. The corresponding
 470 vertical profiles of various aerosol species including sulfate, dust, sea salt, black carbon, and
 471 total organic carbon are shown in Supplementary Figure S3 (panel a-e). The corresponding
 472 IMPROVE measurements are also shown in the same Figure. There were no direct

Deleted: ¶

Deleted: S2

481 measurements of PBAP mass during IMPROVE and therefore it was derived from the
482 measured mass of the total organic carbon (TOC). The relative contribution of insoluble and
483 soluble organic carbon to TOC was assumed to be 20% and 80%, respectively by assuming a
484 water-soluble fraction of 80% for carbonaceous aerosol (Phillips et al. 2017b). AC takes into
485 account the soluble fraction of each type of aerosol. The values of this factor are 0.15 for
486 dust, and 0.8 for carbonaceous species. The value of this fraction for all PBAP groups is 0.1.

487 There are very few observations available in the literature showing the fraction of
488 PBAP in the insoluble organics or total aerosol particles. For example, observations by
489 Matthias-Maser et al. (2000) found that 25% of the total insoluble particles are biological.
490 PBAPs can contribute a significant fraction to the number concentrations of total aerosol
491 particles (Matthias-Maser et al., 1999). Matthias-Maser and Jaenicke (1995) showed that
492 PBAPs can amount to 20% and 30% of the total aerosol particles. The observation by
493 Jaenicke (2005) in a semi-rural location showed that cellular particles can contribute up to
494 about 50% of total particles. Based on these studies we assumed that 50% of the insoluble
495 organics were biological in origin. The total PBAP loading was prescribed partly based on
496 observations of insoluble organics. The mass fraction of each PBAP group in total PBAP
497 mass is prescribed based on the PT21 observations. The fraction of mass mixing ratio for
498 various PBAP groups is: FNG= 0.39, BCT= 0.13; PLN= 0.31; DTS= 0.17; ALG= $2.5 \times$
499 10^{-4} .

Deleted: ¶

500 It should be noted that the observations of PBAPs over different geographical
501 locations (including the region where we carried out the simulation) are rare, which prevents
502 us from using the region-specific PBAP observations for the present study. Hence, PT21's
503 default observations were used to calculate the relative contribution of various PBAP groups
504 to insoluble organics. The parameters for the shape of PSD of each PBAP group (modal mean

Deleted: ¶

507 diameters, standard deviation ratios, and relative numbers in various modes) are prescribed
508 based on observations from Amazon (PT21). Supplementary Figure S4 depicts the
509 corresponding size distribution of various PBAP groups in AC. To check the validity of the
510 observation from PT21 over the region considered in the current study, the model estimated
511 values of one of the major PBAP bacteria are compared with the observations as shown in
512 Supplementary Figure S5. It shows that the estimated values of bacterial number
513 concentration are overall in fair agreement with previous observations (e.g. Bowers et al
514 2009; Bauer et al. 2002; Burrows et al. 2009). The simulated bacterial ($\sim 10^4 \text{ m}^{-3}$) and fungal
515 ($\sim 10^3 \text{ m}^{-3}$) number concentration by AC is in good agreement with their typical
516 concentration in the atmosphere (Després et al. 2012). The resulted vertical profiles of mass
517 of the various PBAP groups are shown in Figure S3 (panel f).

518 From these prescribed loadings of aerosol species, AC predicts their size distribution
519 and hence the CCN activity spectrum. Using the initial sounding and aerosol profile, AC can
520 predict the in-cloud size distribution of aerosols in each species as well as in-cloud
521 supersaturation. Figure S6 in Supplementary Information shows the predicted CCN spectrum
522 comparison with observations from the CCN counter at the surface at the SGP site. It should
523 be noted that the aerosol mass loading from IMPROVE observations showed variations of
524 20-30% for the simulated case. The uncertainties in the input aerosol mass loading can result
525 in simulated CCN concentration and are shown by the errors in the CCN concentration
526 predicted by the AC. During 19-20 May, the measured number concentration of active CCN
527 at the SGP CF ranged from 400 to 3000 cm^{-3} at 1% supersaturation (Fridlind et al. 2017). The
528 measurements were made on 20 May before the start of the rain in clear air. The normalized
529 CCN number concentrations at 1% supersaturation from observations and AC are $\sim 1000 \text{ cm}^{-3}$
530 3 and $\sim 940 \text{ cm}^{-3}$, respectively. Given the wide range of observed CCN concentrations at each

Deleted: S3

Deleted: The figure depicts unimodal size distribution for FNG, BCT, PLN, and ALG, whereas DTS has a bimodal size distribution. ...

Deleted: S4

Deleted: S2

Deleted: ¶

Deleted: To validate this prediction,

Deleted: 2

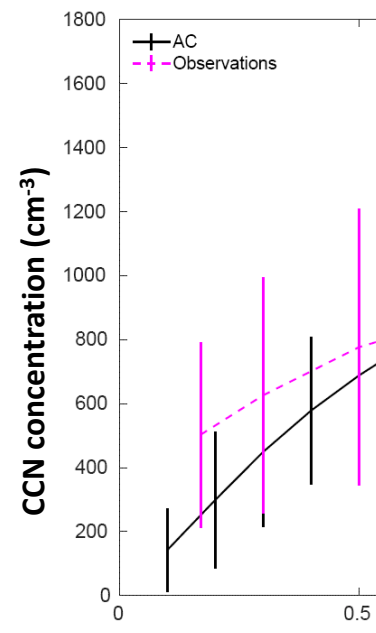
Deleted: ed

Deleted: ¶

Deleted: ¶

Deleted: ¶

Deleted: ¶



Deleted: Figure 2. The CCN spectrum from AC for a simulated squall line case on May 20, 2011, for an environment 500 meters above MSL. The predicted CCN spectrum is compared to the observed CCN spectrum at the SGP CF (300 m above MSL). The error bars on the model predicted CCN concentration are associated with uncertainties in the input values of mass mixing ratios of various aerosol species that act as CCN. ¶


554 supersaturation as well as the uncertainties in the model predicted CCN concentration, the
555 predicted and observed CCN activity spectra are in acceptable agreement.

556  Deleted: ¶

557 4. Results from control simulation and model validation

558 4.1 Overview of the control simulation

559 An intense north-to-south oriented squall line moved over the ARM SGP CF on May 20,
560 2011, from 1100 to 1400 UTC (Sec. 2.1). The new version of AC simulated this case, after
561 implementing the empirical formulation by PT21 for multiple groups of PBAP INPs
562 ('control' simulation) (Sec. 3). It should be noted that five ensemble runs were carried out for
563 control simulation (See Table [S3 in Supplement Information](#)) varying the perturbing in the
564 initial water vapor mixing ratio.

565  Deleted: ¶

566  Deleted: 3

567 cloudy regions. The maximum average cloud droplet number concentration was around 250
568 cm^{-3} . The LWC was typically less than 0.5 g m^{-3} . The freezing level (0°C) was around 4.1
569 km above MSL. The deep convection began around 10 UTC, followed by intense
570 precipitation around 11 UTC, and reached its peak around 12 UTC. The time-height
571 evolution of cloud ice, snow, and graupel number concentrations shows maxima shortly
572 before 12 UTC, which coincides with the time of peak precipitation. This suggests that the
573 ice phase was important in precipitation formation.

574  Moved (insertion) [1]

575  Deleted: 3

576 The time-height map of simulated radar reflectivity during 20 May, unconditionally
averaged over the whole domain is shown in Figure 1g. It shows the well-defined squall line
passing over the domain from 1100 to 1500 UTC. The maximum of this domain-wide

simulated reflectivity is around 40 dBZ, when deep convection was happening. The instantaneous maximum of reflectivity at any grid-point (not shown here) was about 50 dBZ. At other times, the average reflectivity was typical of the stratiform cloud of about 15 dBZ. The cloud top height of the squall line decreases after 1400 UTC.

Deleted: (Fig. 3d)

Deleted: At

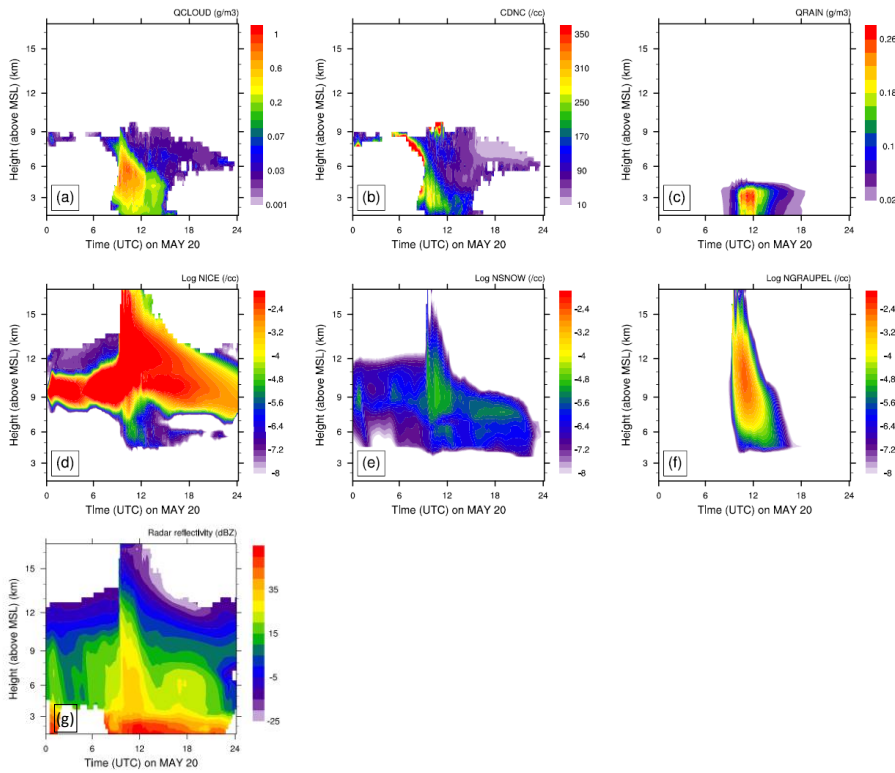


Figure 1: Time-height contours of domain averaged a) cloud water mixing ratio (QCLOUD); b) cloud droplet number concentration (CDNC); c) rainwater mixing ratio (QRAIN); d) number concentration of cloud ice (NICE); e) number concentration of snow (NSNOW); f) number concentration of graupel (NGRAUPEL). Due to a wide range of values, the log values number concentrations are plotted. The surface height is ~ 500 m. The averaging was done for cloud points with LWC > 0.001gm⁻³ or total water content (TWC) > 10⁻⁶ gm⁻³. Also shown is the time-height evolution of domain averaged (g) radar reflectivity.

Deleted: 3

4.2. Model validation against coincident observations of the storm

The extended stratiform region of the squall line while in the vicinity of the SGP CF was sampled by the Citation aircraft equipped with a full suite of cloud microphysical instrumentation. The aircraft started sampling the stratiform precipitation region at around 1300 UTC and continued the observations at sub-freezing temperatures from 1335 to 1515 UTC. Occasionally, the aircraft encountered weak convective updrafts (< 6 m/s). The aircraft actively avoided convection that was more vigorous than that. In this section, we validate various microphysical and dynamical quantities from the control simulation against aircraft and ground measurements. The control run includes all primary and SIP processes of ice initiation. The vertical profiles shown here are an average of five ensemble runs.

Figure 2 compares the aircraft observations against predicted microphysical quantities, with both the predictions and observations identically averaged, conditionally over convective ($6 > |w| > 1$ m/s) and stratiform regions ($|w| < 1$ m/s). The simulated LWC decreases exponentially with height above the cloud base. There is considerable scatter in observed LWC at each level. The various degrees of dilution of sampled parts of the cloud can cause these variations in LWC at a given altitude. The maximum simulated LWC of 0.5 gm^{-3} was observed in the convective region at temperatures warmer than -5°C . In the convective region around -5°C , the measured LWC is lower than the simulated LWC by a factor of 3. For the stratiform region, simulated values of LWC are in adequate agreement with observations. Overall, the means of observed LWC are in acceptable agreement with the model results for convective as well as stratiform regions.

The vertical profiles of simulated and observed Cloud Drop Number Concentration (CDNC) (Fig. 2c and 2d) showed that CDNC was lower than 300 cm^{-3} . In the convective region, the measured CDNC is 40% lower than the simulated CDNC at 15°C . However, an

Moved up [1]: The time-height map of simulated radar reflectivity during 20 May, unconditionally averaged over the whole domain is shown in Figure 3g. It shows the well-defined squall line passing over the domain from 1100 to 1500 UTC. The maximum of this domain-wide simulated reflectivity is around 40 dBZ (Fig. 3d) when deep convection was happening. The instantaneous maximum of reflectivity at any grid-point (not shown) was about 50 dBZ. At other times,

Deleted: The time-height map of simulated radar reflectivity during 20 May, unconditionally averaged over the whole domain is shown in Figure 3g. It shows the well-defined squall line passing over the domain from 1100 to 1500 UTC. The maximum of this domain-wide simulated reflectivity is around 40 dBZ (Fig. 3d) when deep convection was happening. The instantaneous maximum of reflectivity at any grid-point (not shown) was about 50 dBZ. At other times,

Deleted: n (Sec. 2)

Deleted: ¶

Deleted: 4

Deleted: ¶

Deleted: 4c

Deleted: 4d

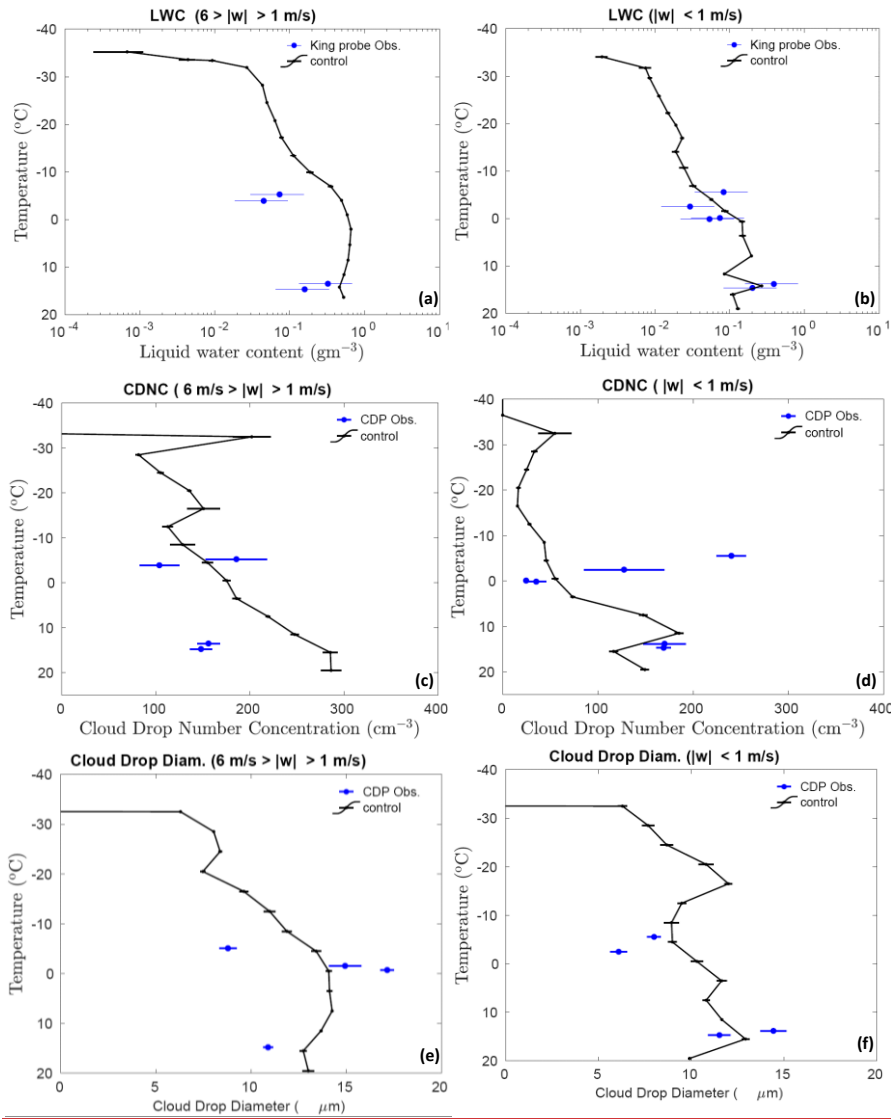


Figure 2: Comparison of the control simulations by AC with aircraft observations, for liquid water content conditionally averaged over (a) convective ($6 \text{ m/s} > |w| > 1 \text{ m/s}$) and (b) stratiform ($|w| < 1 \text{ m/s}$) regions; cloud drop number concentration over (c) convective and (d) stratiform regions; average size of cloud droplets ($< 20 \mu\text{m}$) conditionally averaged over (e) convective and (f) stratiform regions. All the vertical profiles shown here are averaged for the whole domain. The error bars were estimated based on five ensemble runs.

adequate agreement between them is found around -5°C. For the stratiform region, simulated CDNC is much higher in the mixed-phase region. However, at a temperature warmer than 0°C the values of observed CDNC are in acceptable agreement with observations. The observed and simulated mean diameter of cloud droplets varied between 6 to 16 µm (Figures 2e and 2f). There are few points in the convective region e.g., around -5°C, where the observed cloud drop diameter is 50% lower than the simulated value. An adequate agreement between simulated and observed cloud drop diameter was found for the stratiform region. Overall, the predictions of average CDNC and cloud droplet diameter, in both convective and stratiform regions, show a fair agreement with observations.

The ice particle number concentration from observations and the control simulation is also compared as shown in Figures 3a and 3b for convective and stratiform regions, respectively. It should be noted that the observed number concentration of ice particle particles smaller than 200 µm is prone to shattering, even with the use of the shattering correction algorithm. This can introduce a significant bias in the observed ice number concentration (Korolev et al., 1991). To avoid these biases, we have compared the number concentration of ice particles with a diameter greater than 200 µm from both observation and model (denoted by 'NT200'). However, in the rest of the manuscript (in sensitivity studies), the number concentration from the model included ice particles of all size ranges.

Observations show that the concentration of ice particles gradually increases as the temperature decreases, as expected. The maximum ice number concentration from the aircraft observations (with $D > 200 \mu\text{m}$) is $\sim 0.06 \text{ cm}^{-3}$ around -15 °C. Good agreement to within 50% at most levels, was found between the model simulated NT200 and that observed for the convective region.

Deleted: 15

Deleted: over height

Deleted: 4e

Deleted: 4f

Deleted: ¶

Deleted: 5a

Deleted: 5b

Moved (insertion) [2]

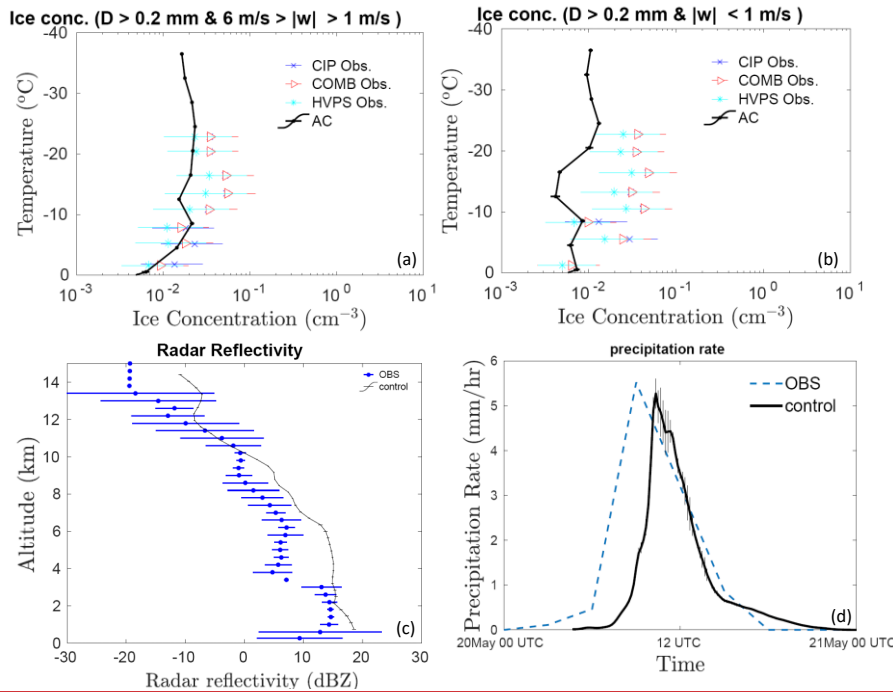


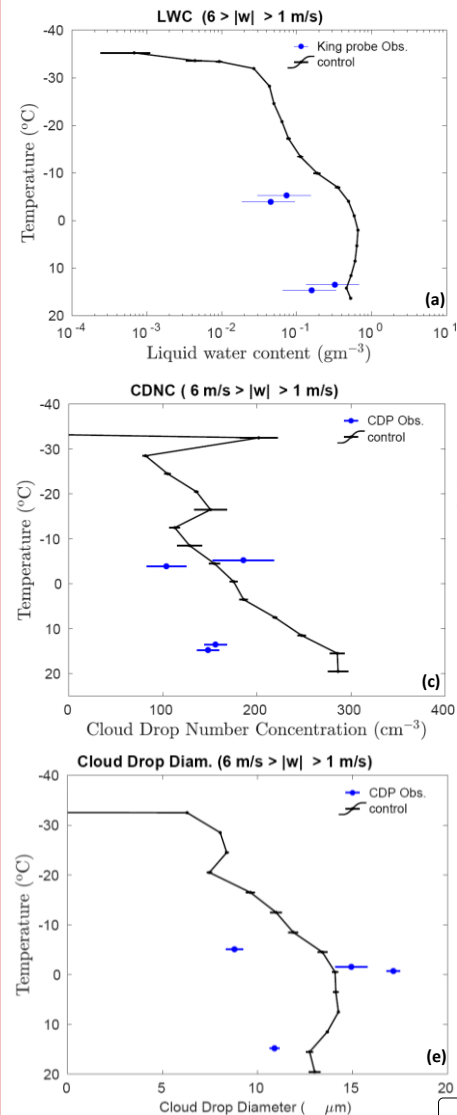
Figure 3: Comparison of the control simulations by AC with aircraft observations, for ice number concentration of all particles > 0.2 (NT200) mm in the maximum dimension of all microphysical species (cloud ice, graupel/hail, snow), averaged over (a) convective ($6 \text{ m/s} > |w| > 1 \text{ m/s}$) and (b) stratiform ($|w| < 1 \text{ m/s}$) regions. (c) The vertical profile of simulated radar reflectivity conditionally averaged over all regions of significant reflectivity ($> -20 \text{ dBZ}$) at each level is compared with observations from ground-based radars. The temperature corresponding to each altitude is mentioned on the right axes: (d) predicted precipitation rate (mm/hr) compared with ground observations at the SGP CF. All the vertical profiles shown here are averaged for the whole domain. The error bars were estimated based on five ensemble runs.

In the stratiform region, at most levels, model values of NT200 have the same order of magnitude as observations. However, between about the -10 and -16°C levels, the stratiform NT200 values are about half an order of magnitude lower than the observations. In similar simulations of the 20 May case, Fan et al. (2015) and Fridlind et al. (2017) also showed underestimation of simulated ice number concentrations. Compared to observations,

Deleted: ¶

Moved up [2]: Observations show that the concentration of ice particles gradually increases as the temperature decreases, as expected. The maximum ice number concentration from the aircraft observations (with $D > 200 \mu\text{m}$) is $\sim 0.06 \text{ cm}^{-3}$ around -15°C . Good agreement to within 50% at most levels, was found between the model simulated NT200 and that observed for the convective region.¶

Deleted:



Deleted: ¶

724 their simulations showed half an order of magnitude bias in ice crystal number concentration.
 725 Comparatively, for the convective region, our model predicted ice number concentrations
 726 were in better agreement with observations. As mentioned in section 2.2, imaging probe data
 727 is prone to shattering, and various corrections were used to rectify it. However, there are
 728 currently no ways to determine how many undetected artifacts remain after shattering
 729 corrections have been applied (Baumgardner et al. 2022). Such uncertainties in measured ice
 730 number concentration could result in such bias in observed and simulated ice number
 731 concentrations. In summary, though the AC model is not totally perfect, it did a fair job in
 732 simulating observed ice number concentrations.

733 In Figure 3c, the radar reflectivity from vertically pointing Ka-band ARM zenith radar
 734 is compared with the mean profile from model simulations. This figure illustrates that
 735 simulated reflectivity profiles below roughly 3 km and above 8 km MSL altitudes are in good
 736 agreement with observations. Between 3 and 8 km MSL (temperatures of 2 and -30°C), the
 737 bias in reflectivity from model simulations and observations is about 10 dBZ. Thus, the
 738 simulated reflectivity is substantially higher than observed, particularly at levels where the
 739 aircraft sampled the clouds. Fridlind et al. (2017), as well as Fan et al. (2015), noticed similar
 740 overestimations of reflectivity within stratiform outflow of the squall line case on 20 May.
 741 They attributed the reflectivity biases to significantly larger ice particles in the simulations
 742 than observed.

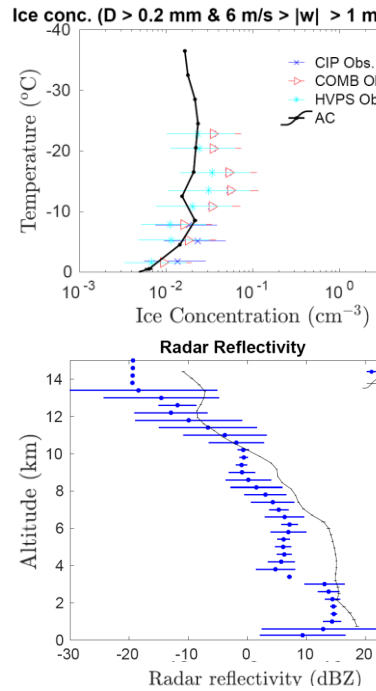
743 Figure 3d compares the time series of precipitation rate from the control simulation
 744 with the radar-based precipitation estimates. In both, control simulation and observations, a
 745 maximum precipitation rate of about 5 mm/hr was noticed, with an error in the prediction of
 746 less than 5%. In comparison to observations, the simulated squall line arrives 1-2 hours later.
 747 The lack of resolution of the 3D turbulence in the planetary Boundary Layer and uncertainties

Moved (insertion) [3]

Deleted: 5

Moved up [3]: In Figure 5c, the radar reflectivity from vertically pointing Ka-band ARM zenith radar is compared with the mean profile from model simulations. This figure illustrates that simulated reflectivity profiles below roughly 3 km and above 8 km MSL altitudes are in good agreement with observations. Between 3 and 8 km MSL (temperatures of 2 and -30°C), the bias in reflectivity from model simulations and observations is about 10 dBZ. Thus, the simulated reflectivity is substantially higher than observed, particularly at levels where the aircraft sampled the clouds. Fridlind et al. (2017), as well as Fan et al. (2015), noticed similar overestimations of reflectivity within stratiform outflow of the squall line case on 20 May. They attributed the reflectivity biases to significantly larger ice particles in the simulations than observed. ¶

Deleted: ¶



Deleted: ¶

Figure 5: Comparison of the control simulations by AC with aircraft observations, for ice number concentration of all particles > 0.2 (NT200) mm in the maximum dimension of all microphysical species (cloud ice, graupel/hail, snow), averaged over (a) convective (6 m/s > |w| > 1 m/s) and (b) stratiform (|w| < 1 m/s) regions. (c) The vertical profile of simulated radar reflectivity conditionally averaged over all regions of significant reflectivity (> -20 dBZ) at each level is compared with observations from ground-based radars. The ...

Deleted: ¶

Deleted: 5d

797 associated with the 3D structure of initial and boundary conditions can all have an
798 independent impact on the simulated rainfall structure, resulting in a delayed peak.
799 Nonetheless, AC has done a fair job in simulating the peak in the predicted precipitation rate.

800

801 *4.3 Analysis of simulation with ice particle budgets and tagging tracers*

802 The activated PBAP INPs from the control run are shown in Figure 4 for the convective and
803 stratiform regions. In addition to the PBAP INPs, Figure 4 also shows the activated INPs
804 from dust and black carbon. It should be noted that these concentrations shown here are based
805 on advective tagging tracers that follow the diffusion, ascent, and descent inside cloud
806 motions. Overall, bacterial, and fungal particles dominate the biological INP concentration in
807 the simulated cloud. For example, at -20°C the activated INPs from bacteria and fungi are
808 higher than the other three groups of PBAP INPs (detritus, pollen, algal) by two orders of
809 magnitude in both convective as well as stratiform regions. At that level in convective
810 regions, the average concentration of simulated active PBAP INPs is about $3 \times 10^{-6} \text{ cm}^{-3}$,
811 which is two orders of magnitude less than the maximum total for all active INPs (about
812 $3 \times 10^{-4} \text{ cm}^{-3}$) in the whole simulation. Overall, the predicted total INP concentration is
813 dominated by black carbon and dust. At -10°C, the Activated INPs from dust and black
814 carbon differ by an order of magnitude from the total PBAP INPs in convection.

Deleted: 6

Deleted: 6

Deleted:

818

819

824

825

826

827

828

829

830

831

832

833

834

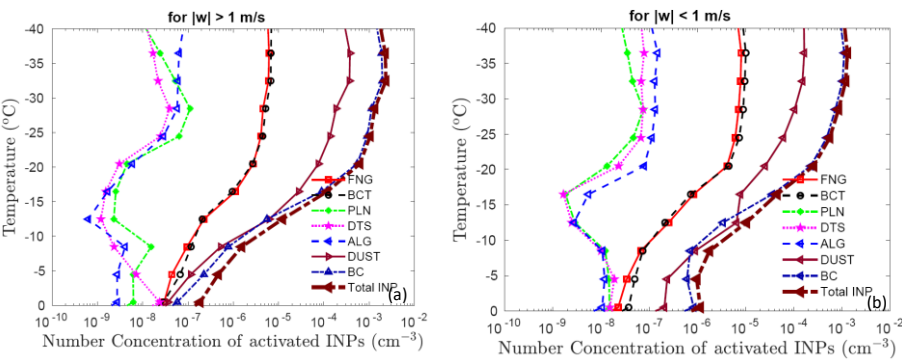


Figure 4: The activated number concentration INPs from various PBAP groups along with dust (DUST) and black carbon (BC) and total INPs at various temperatures for (a) convective and (b) stratiform regions. All the vertical profiles shown here are averaged for the whole domain.

The formation of ice in a cloud is a result of several primary and secondary processes.

It is important to understand the relative importance of these processes in precipitation formation. To that end, Figure 5a shows the ice particles initiated from various sources throughout the 3D domain of the entire simulation. The primary homogeneous (PRIM_HOM) dominates the total ice budget. Among all SIP mechanisms, breakup caused by collisions between various ice particles is the most important in determining total ice number concentration. The ice production by sublimation breakup of graupel is slightly lower than PRIM_HOM. However, the contribution of ice production via sublimation breakup of dendritic ice crystals is negligible.

Deleted: 6

Deleted: ¶

Deleted: 7a

Moved (insertion) [4]

Formatted: Indent: First line: 1,27 cm

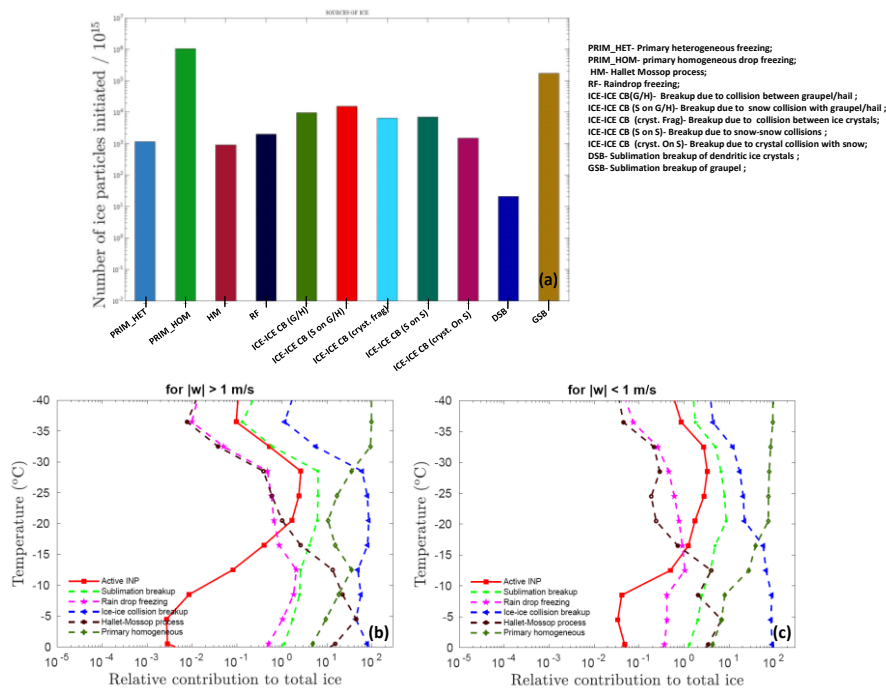


Figure 5: (a) Ice crystal budget for simulated MC3E case. The number of ice crystals produced by various mechanisms (as shown in the legend box) per 10¹⁵ particles is shown. Also shown is the relative contribution of various SIP mechanisms such as sublimation breakup, raindrop freezing, ice-ice collision breakup, and the Hallett-Mossop process to the total ice number concentration as a function of temperature, averaged conditionally over only (b) convective and (c) stratiform regions. The relative contribution was calculated based on advective tagging tracers for the given process. The convective and stratiform regions were identified based on criteria $|w| > 1$ and $|w| < 1$, respectively.

Figure 5b and 5c depict the relative importance of ice concentration from various SIP mechanisms, as well as active INPs in determining total ice number as a function of temperature for convective and stratiform regions. Each source of ice displayed is tracked with advective “tagging tracers” throughout the simulation. Overall, at temperatures warmer than -15°C, the contribution to the total ice number concentration from various SIP is 2-3

Deleted: ¶

Deleted: 7

Moved up [4]: The primary homogeneous (PRIM_HOM) dominates the total ice budget. Among all SIP mechanisms, breakup caused by collisions between various ice particles is the most important in determining total ice number concentration. The ice production by sublimation breakup of graupel is slightly lower than PRIM_HOM. However, the contribution of ice production via sublimation breakup of dendritic ice crystals is negligible.¶

Deleted: ¶

Deleted: 7

Deleted: 7c

orders of magnitude higher than the concentration of active INPs, highlighting the importance of SIP mechanisms in ice formation. At -25°C, breakup in ice-ice collisions contributes around 75% and 20% of the total ice concentration in the convective and stratiform regions, respectively. At the same temperature, in both convective and stratiform regions, sublimation breakup and raindrop freezing contribute about 8% and 0.8 %, respectively. It can be observed that in the convective regions at temperatures warmer than -30°C, SIP mechanisms are important in determining the total ice concentrations, whereas at colder temperatures homogeneous nucleation is dominant. In the stratiform region, this crossover occurs at a much warmer temperature around -18°C. At temperatures colder than this homogeneous nucleation is a major contributor to the total ice whereas at warmer temperatures SIP mechanisms prevail. Overall, the contribution of active INP to the total ice is lower than 3%.

Secondary ice formation via the HM process of rime-splintering contributes significantly to ice production at temperatures warmer than about -15 °C (Fig. 5b and 5c), enhancing the ice concentration beyond the primary ice. In the convective region, the contribution of the HM process in total ice can reach as high as 40% around -5°C. The simulated cloud droplet diameter is mostly smaller than 15 µm. It is smaller than the cloud droplet size required for the HM process to occur. In AC, the rate of the rime-splintering mechanism depends on the concentration of droplets > 24 µm. It should be noted that in the AC model HM process is treated with a factor multiplying the fragment emission which depends on the cloud droplet size. This factor is zero for cloud diameter below 16 µm and unity above 24 µm with linearly interpolated in between.

889

5. Results from sensitivity tests about the influence of PBAP

Deleted: ¶

Deleted: 7

Deleted: 7c

894 To quantify the effect of multiple types of PBAPs on cloud properties, sensitivity tests were
895 performed by modifying the control simulation and comparing the perturbed simulations with
896 it. Description of various sensitivity tests carried out in the current study are enlisted in
897 Supplementary Information (Table S3). The corresponding figures for each simulation are
898 also mentioned.

900 Simulations were performed by eliminating all PBAPs from the control (*'no-PBAP'*
901 case) and by multiplying their initial loadings at all levels by factors of 10 and 100 (*'high-*
902 *PBAP'* and *'very high-PBAP'* cases) respectively. Comparison with the control simulation
903 reveals the overall effect from both the CCN and IN activities of all bioaerosols combined.
904 These factors are justified by considering the variations in PBAP concentrations in the range
905 of about 0.1 to 30 L⁻¹ over North American forests (Huffman et al. 2013). An additional
906 simulation was conducted with a 1000-fold increase in initial PBAP loading (*'ultra high-*
907 *PBAP'*) to investigate if these unrealistically high concentrations of PBAPs could affect the
908 ice phase in a purely hypothetical scenario. Five ensemble runs were carried out for all major
909 simulations involving perturbations in PBAP loading. The ensemble runs were carried out by
910 varying the perturbation in initial conditions (water vapor mixing ratio).

911 Additional simulations were performed by removing treatment of biological IN
912 activity in the EP (*'no-PBAP INP'* case) relative to the control run. A comparison of both
913 additional simulations against the corresponding simulations with the full change in the
914 PBAP loadings (no-PBAP and high-PBAP cases) reveals the separate roles of the INP and
915 CCN activities for the changes in biological material. Apart from these changes in PBAPs,
916 the perturbed simulations are identical to the control run.

917 Figure 6 reveals the effects of all bioaerosols on cloud properties in the convective
918 region ($|w| > 1$ m/s). Overall, changes in cloud microphysical properties including liquid
919 water content, cloud droplet size, cloud drop number concentration, ice number concentration

Deleted: Table 3: Description of various sensitivity simulations carried out in the current study. The corresponding figures for each simulation are also mentioned.

¶ Simulation

Formatted: Indent: First line: 1,27 cm

Deleted: ¶

Deleted: ¶

Deleted: 8

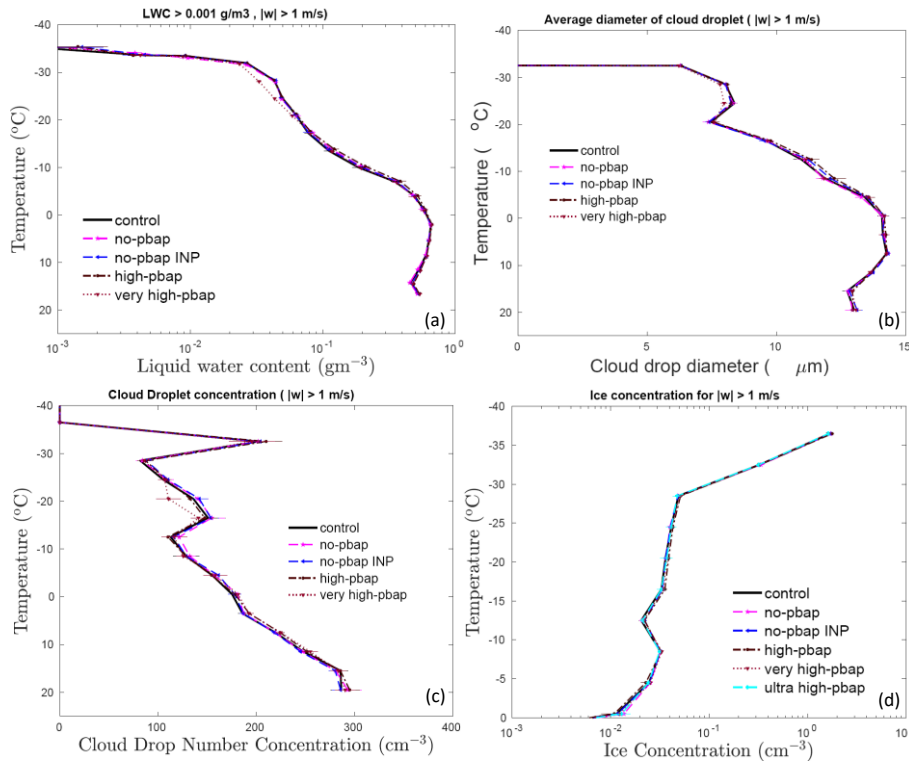


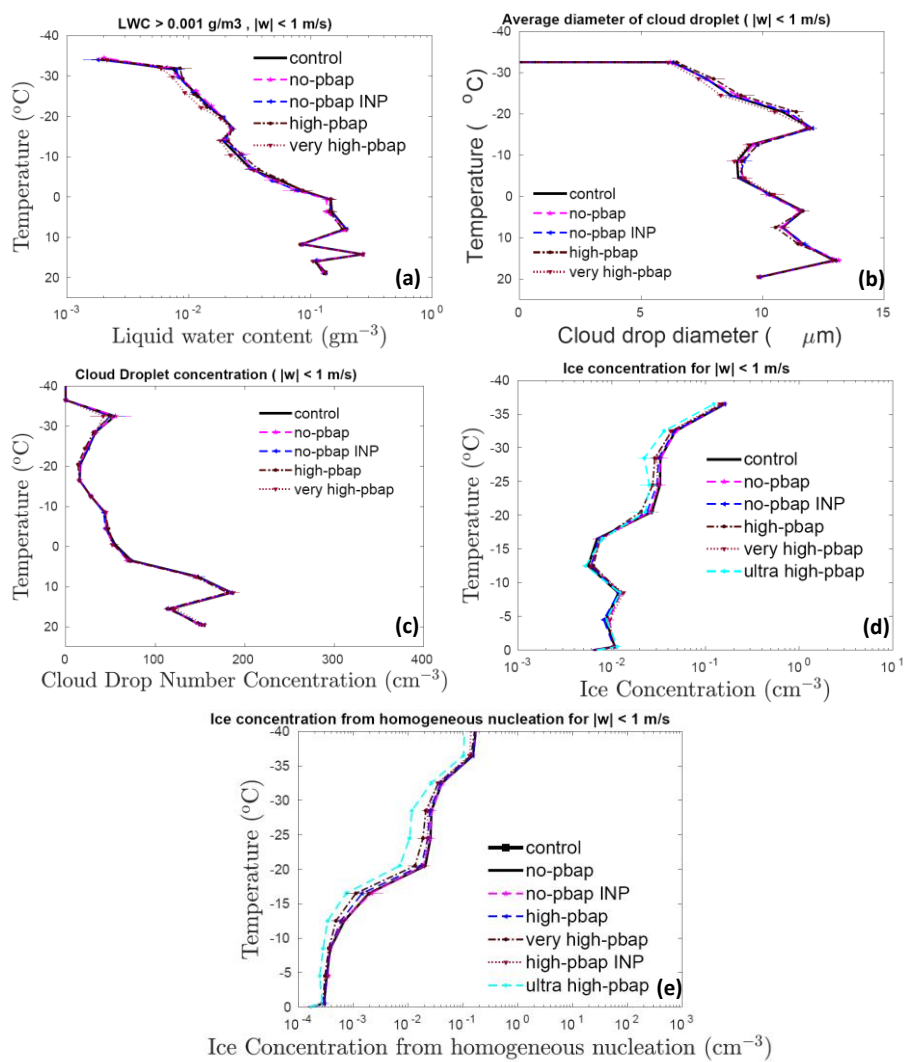
Figure 6: The temperature dependence of the (a) liquid water content, the (b) cloud droplet number, (c) the cloud droplet diameter, and the (d) total ice number concentration for ‘control’ simulation and various sensitivity runs involving a change in total PBAP number concentrations for in the convective region. The averaging conditions are mentioned at the top of each figure. The ice number concentration from the ultra high-PBAP is also shown in panel d. All the vertical profiles shown here are averaged for the whole domain.

are less sensitive to the changes in PBAPs for the convective part of the simulated clouds and are not statistically significant. The LWC, cloud droplet number and cloud drop diameter in the perturbed simulations does not differ much ($< 3\%$) from the control run. For the whole storm, considerable changes in the spatial distribution of total ice number concentration are observed due to changes in PBAPs (see [Supplementary Figure S7](#)). However, vertical profiles showed very small changes in the ice number concentrations. In the convective region,

Deleted: S5

943 changes in ice crystal number concentration due to changes in PBAPs are negligible ($< 6\%$).

944 This includes the extreme changes in bioaerosol loading (ultra high-PBAP case).



945
946 **Figure 7:** The temperature dependence of (a) the liquid water content, (b) the cloud droplet
947 number, (c) the cloud droplet diameter, and the (d) total ice number concentration for
948 'control' simulation and various sensitivity runs involving a change in total PBAP number
949 concentrations for in the stratiform region. Also shown is the temperature dependence of (e)
950 ice concentration from homogeneous freezing. The averaging conditions are mentioned at the

951 top of each figure. The total ice number concentration and ice number from homogeneous
952 freezing from ultra high-PBAP are also shown in panels d and e. All the vertical profiles
953 shown here are averaged for the whole domain. The error bars are based in ensemble runs.

954

955 Figure 7 shows the corresponding effects in the stratiform region ($w < 1$ m/s) from
956 all bioaerosols. The changes in warm microphysical properties because of changes in PBAP
957 loadings are smaller than 10%. In this part of the cloud, the ice-microphysical parameters are
958 comparatively more sensitive to the changes in PBAP than in the convective region. The ultra
959 high-pbap case predicted ~40% lower ice number concentration than the control run.
960 However, these changes in ice number concentration are not significant as the error bars
961 associated with ensemble members overlap. For the stratiform region, all other simulations
962 considered here showed < 10% change in ice number concentrations compared to the control
963 run. These changes in ice number concentration due to PBAPs are mostly controlled through
964 their effect on homogeneous freezing above the -36°C level as shown in Figure 7e by tagging
965 tracer for homogeneous nucleation. These ice particles can then advect to lower levels
966 affecting ice number concentrations in the mixed-phase region.

967

968 Figure 8 shows the number of ice particles generated by homogeneous nucleation,
969 various mechanisms of primary nucleation (8a), and secondary ice production (8b) per 10^{15}
970 ice particles for the entire storm. Homogeneous freezing dominates the ice production among
971 the three broad types of ice formation mechanisms (heterogeneous and homogeneous ice
972 nucleation, SIP). The maximum changes in ice nucleated through the primary ice mechanism
973 are noticed for the very high-PBAP case and can be attributed to the 100-fold increase in all
974 PBAP loading. The very high-PBAP simulation predicted a 15% lower number of
975 homogeneously nucleated ice than the control run. The very high-PBAP cases predicted
976 about 80% more primary ice crystals formed at temperatures warmer than -30°C. At

Formatted: Indent: First line: 1,27 cm

Deleted: 10

Deleted: 10a

Deleted: 10b

temperatures colder than -30°C , this case predicted 20% more primary ice crystals than the control run. The very high pbap case showed an increase in primary heterogeneous ice and a decrease in primary homogenous ice. Since the contribution of primary homogenous ice nucleation is much higher in determining the total ice number concentration when compared with primary homogeneous nucleation, the overall effect of the very high pbap case is a decrease in total ice number concentration as shown in Figure 7 and Table S4 in the Supplementary Information. However, at temperatures warmer than -35°C , ice number concentration in very high pbap case was comparable with the control run (Table S5).

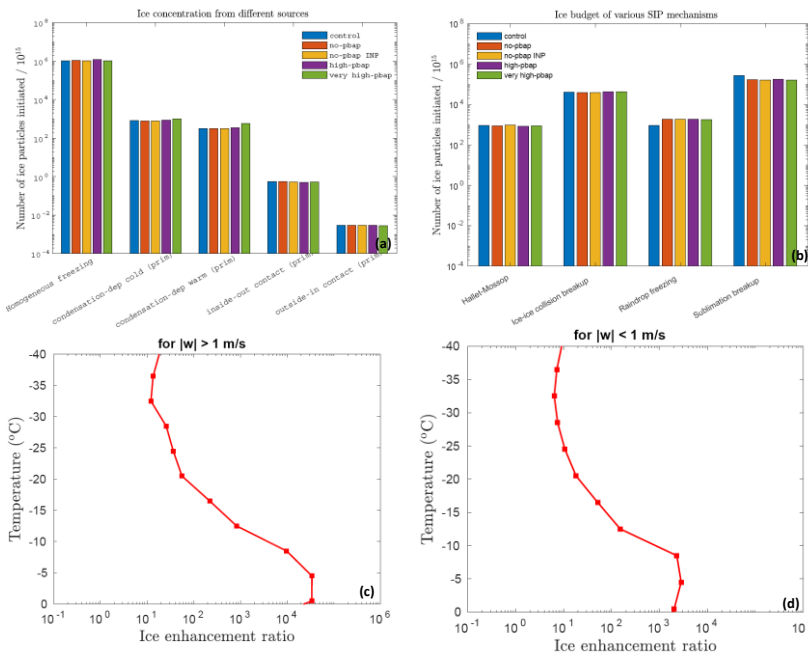
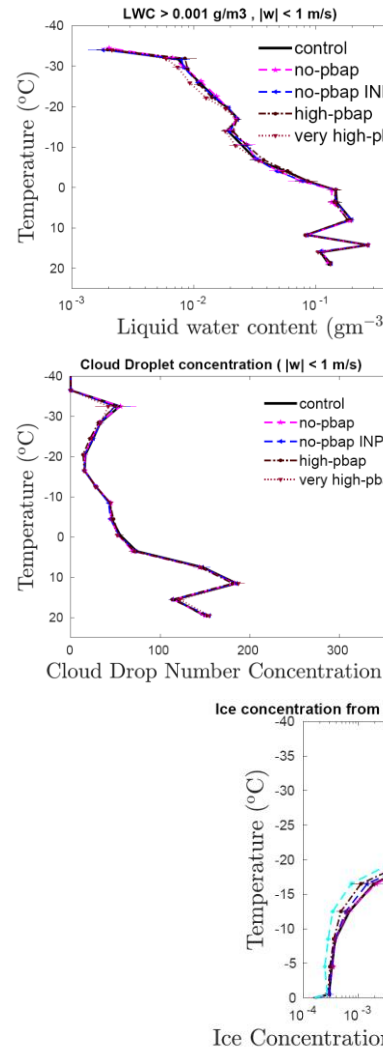


Figure 8: The number of ice crystals produced during the whole storm by (a) primary ice nucleation mechanisms and homogeneous freezing as well as (b) various SIP mechanisms (as shown in the legend box) per 10^{15} particles is shown for various sensitivity runs. The ice enhancement ratio for convective and stratiform region is shown in 8c and 8d.

Deleted: 9

Deleted: 4

Formatted: Superscript



Deleted:

Figure 9: The temperature dependence of (a) the liquid water content, (b) the cloud droplet number, (c) the cloud droplet diameter, and the (d) total ice number concentration for 'control' simulation and various sensitivity runs involving a change in total PBAP number concentrations for in the stratiform region. Also shown is the temperature dependence of (e) ice concentration from homogeneous freezing. The averaging conditions are mentioned at the top of each figure. The total ice number concentration and ice number from homogeneous freezing from ultra high-PBAP are also shown.

Deleted: 10

1024
1025
1026
1027
1028
1029
1030
1031
1032
1033
1034
1035
1036
1037
1038
1039
1040
1041
1042
1043
1044
1045
1046
1047
1048

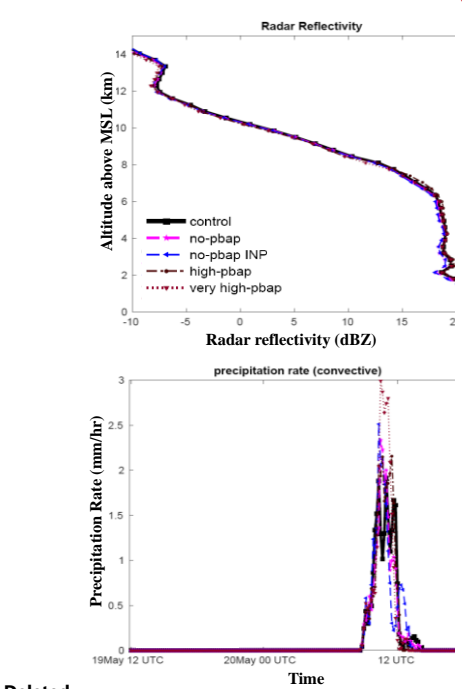
Figure 8b shows that among SIP mechanisms, the contributions of ice-ice collision breakup and sublimation breakup are higher by an order of magnitude than the HM process and raindrop fragmentation. However, the budget analysis (not shown in the plot) showed that about 75% of the fragments associated with sublimation breakup are prone to evaporation, making ice-ice collision breakup a major SIP mechanism. The estimated ice enhancement ratio, which is a ratio between the number concentrations of total ice (excluding homogeneous nucleation) and primary ice, is shown in Figures 8c and 8d for convective and stratiform regions respectively. Overall, the ice enhancement ratio varied between 10 to 10⁴ which indicates the importance of SIP mechanisms. The budget analysis shows that overall, the perturbations in bioaerosols resulted in very small changes (with maximum change < 40%) in ice generated by SIP mechanisms.

The role of PBAPs in altering radar reflectivity and surface precipitation was limited and described briefly in Supplementary material (Figure S8). The overall effect of PBAPs on accumulated surface precipitation was minimal (< 4%) (Figure S8 and Table S4). In addition, the changes in PBAPs do not show a significant impact on shortwave and longwave radiation fluxes as well cloud fractions as discussed in the Supplementary information (Figure S9).

6. Results from sensitivity tests about secondary ice production

Various sensitivity experiments were conducted to evaluate the role of SIP mechanisms in determining micro- and macrophysical parameters of the clouds (See Table S3). SIP through sublimation breakup and breakup in ice-ice collisions were switched off in the 'no-sublimation breakup' and 'no-collisional ice-ice breakup' simulations, respectively. In the 'no-secondary' case, no SIP mechanisms were active.

Deleted: 10b
Formatted: Indent: First line: 1,27 cm
Deleted: 10c
Deleted: 10d
Formatted: Highlight
Deleted: ¶



Deleted:
Figure 11: The vertical profiles of (a) radar reflectivity are shown for simulations involving changes in PBAP. (b) The temporal evolution of the total surface precipitation rate averaged over the domain is also shown. The time series of surface precipitation rate averaged over the domain is also shown separately for (c) convective and (d) stratiform regions. All the vertical profiles shown here are averaged for the whole domain.¶
Figure 11a shows the effects of PBAP on the simulated radar reflectivity for the whole storm. When compared to the control run, there is no significant difference in the simulated radar reflectivity of the perturbed simulations (< 4%). Figure 11b depicts the sensitivity of the total surface precipitation rate averaged over the domain to the changes in total PBAPs. As shown in Figure 11b, the peak in surface precipitation rate is boosted by about 10% in the very high-PBAP cases compared to the control run. In remaining perturbed simulations, changes in surface precipitation rate are less than 5% when compared with the control run. The contribution from the stratiform component of rain is higher in the total amount of rain (90%) as compared to the convective rain (remaining 10%) (see Fig. 11c and 11d). Convective rainfa...

Deleted: ¶

1125 The results from these sensitivity experiments are shown in Figure 9 for the
1126 convective as well as the stratiform region of the simulated cloud. Overall, in the convective
1127 region, the no-secondary and no-collisional ice-ice breakup cases predicted 5 and 12% higher
1128 LWC respectively, than the control run (See Table S4 in Supplementary Information). In the
1129 stratiform region, these cases predicted ~25% higher LWC than the control run. Lower ice
1130 number concentrations due to the absence of SIP mechanisms may reduce the rate of
1131 conversion of liquid to ice via mixed-phase processes, resulting in a higher LWC.

Deleted: ¶

Deleted: 13

Deleted: 4

1132 In the convective part, the absence of any SIP increased ice number concentration by
1133 half an order of magnitude at temperatures warmer than -25°C. Comparing the no-SIP and
1134 control cases, the effect of the inclusion of SIP mechanisms is to increase the average ice
1135 concentration by up to half an order of magnitude at temperatures warmer than -15°C in the
1136 stratiform region. For the stratiform region, at temperatures colder than this, the absence of
1137 SIP mechanisms resulted in higher ice number concentrations by a similar magnitude. These
1138 changes at the colder levels are associated with homogeneous droplet freezing. The changes
1139 in ice number concentration in the no-collisional ice-ice breakup case are comparable with
1140 the no-secondary case. Compared to break up in ice-ice collisions, sublimation breakup has a
1141 lower impact (< 40%) on the total ice number concentration in both convective and stratiform
1142 regions.

Deleted: ¶

Formatted: Superscript

Moved (insertion) [6]

Deleted: ¶

1143 The changes in simulated radar reflectivity, total specific differential phase, and
1144 surface precipitation rate with SIP mechanisms are shown in Figures 9e, 9f, and 9g,
1145 respectively for the whole storm. Overall, the simulated radar reflectivity was 1 dBZ lower in
1146 the no-SIP and no-collisional ice-ice breakup case than in the control run and can be
1147 attributed to the overall increase in ice number concentration in the control run.

Formatted: Indent: First line: 1,27 cm

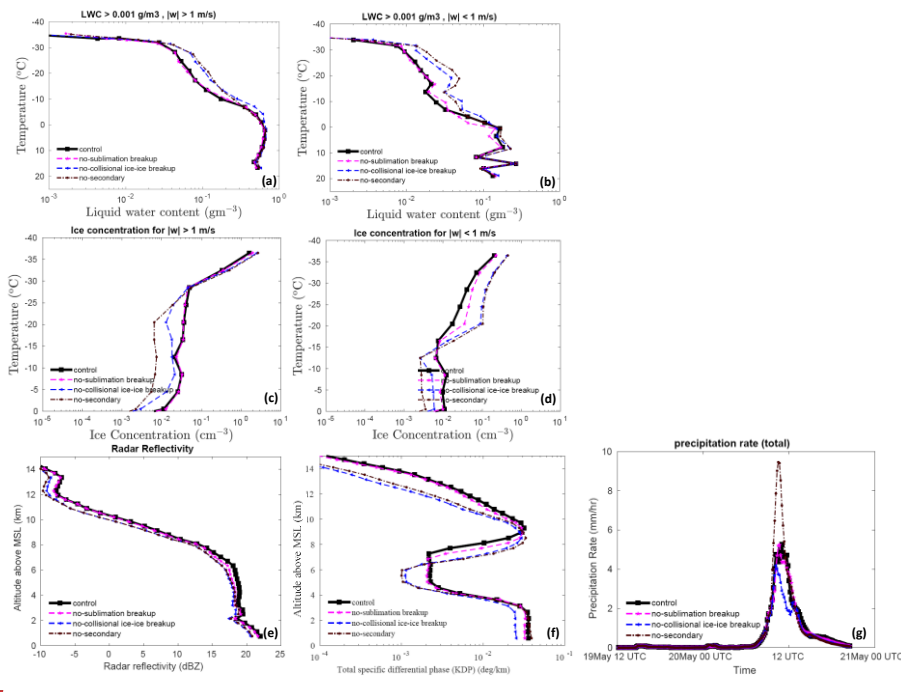


Figure 9: Temperature dependence of the liquid water content in (a) the convective and (b) the stratiform region for ‘control’ simulation and various sensitivity runs involving SIPs. The ice number concentration is also shown for the (c) convective and (d) stratiform regions. The averaging conditions are mentioned at the top of each figure. The vertical profiles of (e) radar reflectivity, (f) total specific differential phase are also shown for the same simulations. (g) The temporal evolution of the total surface precipitation rate averaged over the domain is also shown. All the vertical profiles shown here are averaged for the whole domain.

The no-sublimation case predicted slightly higher reflectivity than the control run.

The absence of all SIPs resulted in about a 100% decrease in the K_{DP} at a temperature colder than -40°C. Between -10°C to -30°C, the absence of no-collisional breakup and no-secondary resulted in higher K_{DP} (half an order of magnitude) values than the control run. The absence of all SIP mechanisms results in a higher surface precipitation rate (75%) during the peak rainfall hour, which occurs around 11.30 UTC compared to the control run. In the previous study, Phillips et al. (2017b) have shown that SIP through ice-ice collision breakup can

Moved (insertion) [5]

Deleted: ¶

Deleted: 13

Moved up [6]: concentration by up to half an order of magnitude at temperatures warmer than -15°C in the stratiform region. For the stratiform region, at temperatures colder than this, the absence of SIP mechanisms resulted in higher ice number concentrations by a similar magnitude. These changes at the colder levels are associated with homogeneous droplet freezing. The changes in ice number concentration in the no-collisional ice-ice breakup case are comparable with the no-secondary case. Compared to break up in ice-ice collisions, sublimation breakup has a lower impact (< 40%) on the total ice number concentration in both convective and stratiform regions.¶

Moved up [5]: ¶

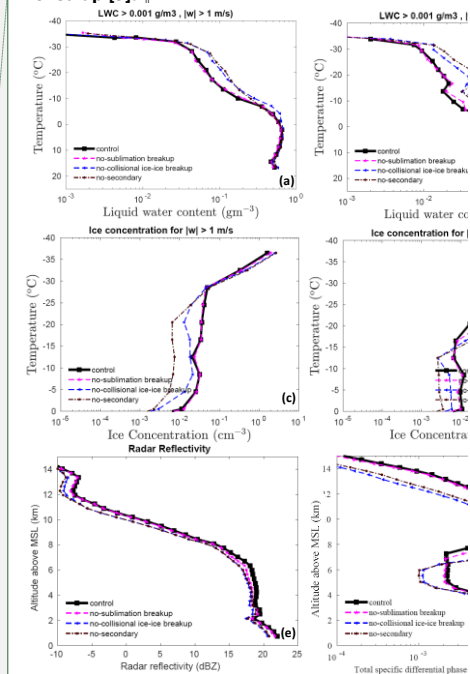


Figure 13: Temperature dependence of the liquid water content in (a) the convective and (b) the stratiform region for ‘control’ simulation and various sensitivity runs involving SIPs. The ice number concentration is also shown for the (c) convective and (d) stratiform regions. The averaging conditions are mentioned at the top of each figure. The vertical profiles of (e) radar reflectivity, (f) total specific differential phase are also shown for the same simulations. (g) The temporal evolution of the total surface precipitation rate averaged over the domain is also shown. All the vertical profiles shown here are averaged for the whole domain.

Deleted: ¶

¶

The changes in simulated radar reflectivity, total specific differential phase, and surface precipitation rate with SIP mechanisms are shown in Figures 13e, 13f, and 13g, respectively for the whole storm. Overall, the simulated radar reflectivity was 1 dBZ lower in the no-SIP and no-collisional ice-ice breakup case than in the control run and can be attributed to the overall increase in ice number concentration in the control run. ...

1213 reduce accumulated surface precipitation in the simulated storm by 20%-40%. They
1214 attributed it to the increase in snow particles competing for available liquid and the reduction
1215 in their growth by riming. It resulted in smaller ice particles and a reduction in surface
1216 precipitation.

1217

1218 **7. Results about the influence of PBAPs in the absence of SIP mechanisms**

1219 To investigate the role of PBAPs in altering cloud microphysical properties through SIP
1220 mechanisms, an additional simulation was performed by eliminating all secondary ice
1221 processes from the control run and multiplying the initial loading of all PBAP groups by a
1222 factor of 100 (the ‘very high-PBAP with no SIP’ case). The results of this simulation are then
1223 compared to the no-SIP case as shown in Figure 10.

1224 In the absence of any SIP mechanisms, the 100-fold increase in bioaerosols resulted in
1225 minimal effect on ice number concentration. Overall, without SIP the increase in bioaerosol
1226 loading by 100-fold resulted in less than a 5% change in ice number concentration. This
1227 indicates that the ice produced by various SIP mechanisms does not alter the effect of
1228 bioaerosols on-ice number concentration in the simulated clouds. The changes in simulated
1229 radar reflectivity due to a 100-fold increase in bioaerosols are negligible (< 0.5%) (Figure
1230 10c). The difference in predicted surface precipitation rate and accumulated precipitation
1231 between very high-PBAP with no-secondary and no-secondary cases was lower than 3%.

Deleted: ¶

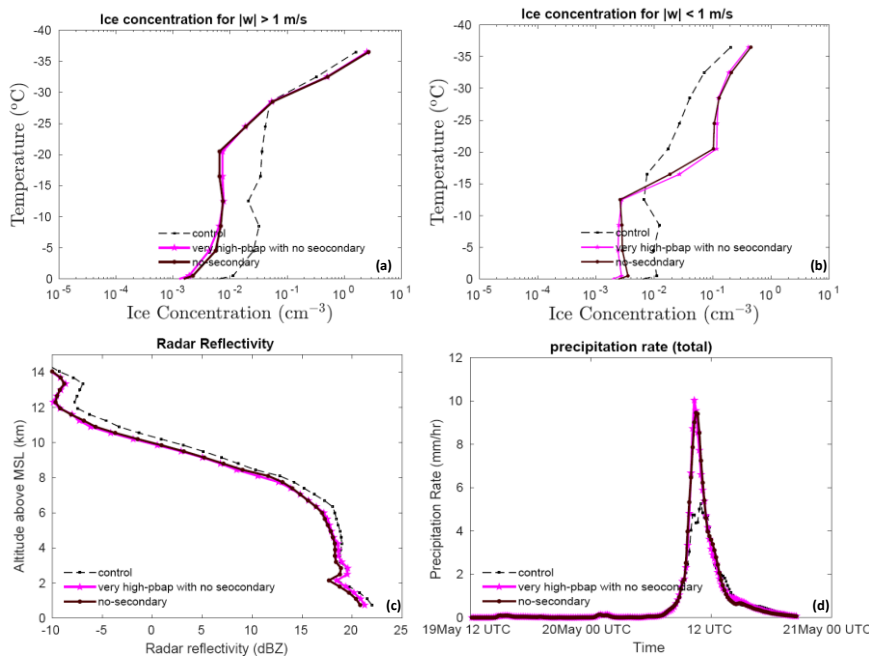
Deleted: Most SIP mechanisms are highly active at temperatures above -15°C. The majority of PBAP showed high ice nucleation activity occurs in this part of the cloud. Most of the ice concentration in this part of the cloud is determined by various SIP mechanisms. Thus, the SIP mechanisms may influence the role of PBAPs in altering cloud microphysical properties. To

Deleted: investigate this aspect

Deleted: 14

Deleted: ¶

Deleted: 4



1244

1245 **Figure 10:** The temperature dependence of ice number concentration for the control, very
 1246 high-PBAP with no SIP and no-SIP simulations averaged for (a) convective and (b)
 1247 stratiform regions. The (c) vertical profile of radar reflectivity and the temporal evolution of
 1248 (d) surface precipitation rate are shown for the entire simulation. All the vertical profiles
 1249 shown here are averaged for the whole domain. All the vertical profiles shown here are
 1250 averaged for the whole domain.

1251

1252 8. Discussion

1253 Five PBAP groups have been implemented in the mesoscale AC model to predict their ice
 1254 nucleation activity based on the empirical formulation by PT21. The simulated concentrations
 1255 of major PBAPs including fungi and bacteria are of the same order of magnitude as results
 1256 from previous modeling studies (Després et al., 2012; Hoose et al., 2010b). Still, the relative
 1257 abundance of PBAP groups over the simulated region is unknown due to the lack of
 1258 measurements. The AC model was run with higher resolution (2 X 2 km) compared to
 1259 previous studies on a global scale (Hoose et al., 2010b), to investigate the potential impact of

Deleted: 14

Deleted: is

Deleted: ¶

1263 variations in PBAP concentration on the properties of simulated squall line events more
1264 clearly.

Deleted: ¶

1265 Yet the control simulation is not perfectly accurate in all respects. In the stratiform
1266 region between -10 and -16°C, the predicted ice number concentration was lower than
1267 observed by aircraft by half an order of magnitude and in fair agreement at temperatures
1268 warmer than -10°C. This uncertainty factor is similar to the uncertainty in the measurements
1269 due to various biases (e.g., Field et al. 2006. Nevertheless, all other simulated cloud
1270 microphysical parameters, radar reflectivity, and surface precipitation rate were in acceptable
1271 agreement with aircraft and ground-based observations.

Formatted: Indent: First line: 1,27 cm

Deleted: a

1272 In the control simulation, the average ice concentration above the -30°C and -18°C
1273 levels is dominated by downwelling of homogeneously nucleated ice from above the mixed-
1274 phase region in convective and stratiform clouds respectively. Below both levels, SIP
1275 prevails. Both processes of ice initiation (homogeneous freezing and SIP) have only weak
1276 sensitivity to PBAPs, hence the weakness of the impact on simulated cloud glaciation.

Deleted: ¶

1277 Based on the sensitivity experiments, it can be concluded that PBAP INPs have only a
1278 limited effect on the average state of the ice phase of the simulated clouds of this mesoscale
1279 convective system. Most of the changes in ice number concentration associated with changes
1280 in PBAPs are controlled by their effects on homogeneous nucleation and SIPs. The lower
1281 dependence of simulated ice number concentration on changes in PBAPs is consistent with
1282 the findings of Hummel *et al.* (2018). Based on ensemble simulations of the regional
1283 atmospheric model for Europe, they showed that the changes in average ice crystal
1284 concentration by biological INPs are very small and are not statistically significant, implying
1285 that PBAPs play only a minor role in altering the cloud ice phase. The limited effect of

Deleted: ¶

1290 PBAPs on cloud properties on a global scale has been highlighted in previous studies (Hoose
1291 et al., 2010b; Sesartic et al., 2012, 2013; Spracklen and Heald, 2014).

1292 The weakness of the simulated impact from realistic PBAP fluctuations is explicable
1293 mostly in terms of the low contribution from biological ice nucleation compared to non-
1294 biological INPs to overall ice initiation. In terms of ice nucleation efficiency and onset
1295 temperatures, each PBAP group has different ice nucleation properties. Based on vertical
1296 profiles of active INPs (Figures 4), the overall contribution of activated INPs from all PBAP
1297 groups to the total active INPs was ~1%. At -15°C, temperature, the active INPs from dust
1298 and black carbon was one order higher than PBAP INPs. At -30°C, the predicted INPs from
1299 dust and black carbon were higher by one and two orders of magnitude, respectively, than
1300 PBAP INPs. The dust and black carbon INPs activated at these temperatures can be advected
1301 down to the levels where PBAP INPs are most important. Overall, this resulted in low
1302 sensitivity of the average ice phase to the changes in bioaerosol loading.

1303 The ice production in the simulated cloud system at levels in the mixed-phase region
1304 (0 to -36 °C) is largely controlled by various SIP mechanisms of which the most important is
1305 the breakup in ice-ice collisions. Some of these processes are active at temperatures warmer
1306 than -15°C (e.g., the HM process) where PBAP INP are important and expected to enhance
1307 the biological ice nucleation. However, our results showed that the ice production associated
1308 with SIP mechanisms is less sensitive to the initial PBAP loading because SIP causes positive
1309 feedback of ice multiplication with ice fragments growing to become precipitation-size
1310 particles that then fragment again.

1311 In our study, a 100-fold increase in PBAPs leads to a < 4% change in surface
1312 precipitation. Using mesoscale model simulations, Phillips et al. (2009) reported a 10%
1313 increase in accumulated surface precipitation associated with deep convective clouds due to a

Deleted: ¶

Deleted: 6

Deleted: ¶

Deleted: ¶

1318 100-fold increase in biological particles. Phillips et al. (2009) also noted an effect (up to 4%)
1319 on surface shortwave and TOA longwave radiation flux because of changes in PBAP number
1320 concentration. In our study, the changes in PBAP loading caused smaller changes in
1321 simulated shortwave and longwave fluxes (< 3%). Sesartic et al. (2012, 2013) showed that
1322 including fungi and bacteria in the global climate model leads to minor changes (< 0.5%) in
1323 the ice water path, total cloud cover, and total precipitation.

1324 It should be noted that the sensitivity experiments carried out in the current study are
1325 limited to the small domain (80 X 80 km domain) representing a limited area of the global
1326 ecosystem. Also, the model top was located at 16 km, and it may not represent the whole
1327 atmosphere. The results presented here are based on a mesoscale model and may not
1328 represent the global impact of PBAPs on clouds.

Deleted: ¶

1329

Formatted: Indent: First line: 1,27 cm

1330 9. Conclusions

Deleted: ¶
¶

1331 A framework describing the ice nucleation activity of five major groups of PBAPs including
1332 fungal spores, bacteria, pollen, viral particles, plant/animal detritus, algae, and their
1333 respective fragments was provided by PT21. The ice nucleation activity of these major PBAP
1334 groups in the EP was based on samples from the real atmosphere. The present study
1335 implements this EP in AC and investigates the role of these five PBAP groups as INPs in
1336 deep convective clouds. The high-resolution (2 km horizontally) simulations over a
1337 mesoscale 3D domain (80 km wide) using AC elucidate the impact of these PBAP groups on
1338 the cloud properties. A series of sensitivity experiments were conducted to test the impact of
1339 PBAP groups on cloud properties.

1340

1344 A mid-latitude squall line that occurred on 20 May 2011 during MC3E over the US
1345 Southern Great Plains is simulated with the model. The simulated number concentration of
1346 ice particles showed good agreement (to within about 50%) with aircraft observations for the
1347 convective clouds within the mesoscale system. In the stratiform region between -10 and -
1348 16°C, the model predicted ice number concentration was lower than the aircraft observation
1349 by half an order of magnitude and in fair agreement at temperatures warmer than -10°C.
1350 Various sensitivity experiments were carried out by perturbing the initial PBAP loading and
1351 by altering various SIP mechanisms.

Formatted: Indent: First line: 1,27 cm

1352 Each PBAP group has diverse properties including its shape, size, and abundance in
1353 the atmosphere. A small fraction of PBAPs is found to be ice nucleation active and can
1354 therefore act as PBAP INPs. The relative contribution of each PBAP within the total PBAPs
1355 may vary from one ecosystem to another. In the current study, their relative contribution is
1356 based on previous observations from Amazonia and can be considered as the main limitations
1357 of this study. However, the simulated number concentrations of major PBAPs including
1358 fungi, and bacteria look reasonable and are close to their typical abundance in the
1359 atmosphere.

Deleted: a

Deleted: ¶

1360 Any perturbation in the PBAP concentration by factors upto 1000 assumed in the
1361 current study (resulted in maximum changes in ice number concentration by < 6% convective
1362 region and by < 40% in the stratiform region with respect to the control run. The simulations
1363 showed that simulated ice particle number concentration is much higher than the number
1364 concentrations of PBAP INPs. Even at temperatures warmer than -15°C, where PBAP INPs
1365 are thought to be the most important INP, ice crystals originated from primary heterogeneous
1366 nucleation of dust and black carbon from higher levels of the cloud frequently perturb the
1367 lower levels due to sedimentation. The major ice formation comes from SIP mechanisms and

1371 homogeneous nucleation, both are less sensitive to the changes in PBAPs. Therefore, PBAP
1372 INPs do not show a significant impact on the average ice phase of the simulated storm.

1373 PBAPs have minimal effect on the warm microphysical properties of simulated
1374 clouds. The effect on liquid water content and cloud droplet number concentration was lower
1375 than 10% in both convective and stratiform regions. Since both ice and warm microphysical
1376 processes are less sensitive to PBAPs, surface precipitation is not affected significantly by
1377 changes in PBAPs. A 100-fold increase in all PBAPs resulted in less than a 5% change in
1378 surface precipitation.

1379

1380 ***Code and data availability:*** Data and the code for the empirical formulation of PBAPs are
1381 available on request by contacting the corresponding author.

1382 ***Competing interests:*** The authors declare no conflict of interest

1383 ***Author Contributions:*** VJTP designed and monitored this study. SP conducted model
1384 simulation, most of the data analysis, and wrote the initial manuscript. All authors contributed
1385 to the scientific discussion and model development.

1386 ***Financial support:*** This work was completed for a sub-award (award number: 2019-26-03)
1387 to VTJP from a US Department of Energy (DoE) direct grant to the Ryzhkov at the
1388 University of Oklahoma (award number: DE-SC0018967). The first author was also
1389 supported by a past award from the Swedish Research Council ('VR'), which concerns
1390 modeling bio-aerosol effects on glaciated clouds (2015-05104) and Sweden's Innovation
1391 Agency (Vinnova; 2020-03406). Other co-authors were supported by a current award from
1392 the Swedish Research Council for Sustainable Development (FORMAS; award number
1393 2018-01795) and US Department of Energy Atmospheric Sciences Research Program (award
1394 number: DE-SC0018932).

Deleted: ¶

Deleted: ¶

¶
¶
¶
¶
¶
¶
¶
¶
¶
¶

References:

Blyth, A. M., Latham, J.: Development of ice and precipitation in New Mexican summertime cumulus clouds. Q. J. R. Meteorol. Soc. 119:91–120, 1993.

Baumgardner, D., Abel, S. J., Axisa, D., Cotton, R., Crosier, J., Field, P., Gurganus, C., Heymsfield, A., Korolev, A., Krämer, M., Lawson, P., McFarquhar, G., Ulanowski, Z., & Um, J.: Cloud Ice Properties: In Situ Measurement Challenges, *Meteorological Monographs*, 58, 9.1-9.23, 2017.

Bowers, R. M., Lauber, C. L., Wiedinmyer, C., Hamady, M., Hallar, A. G., Fall, R., Knight, R., Fierer, N.: Characterization of airborne microbial communities at a high-elevation site and their potential to act as atmospheric ice nuclei. Appl Environ Microbiol. Aug;75(15):5121-30. doi: 10.1128/AEM.00447-09, 2009.

Bauer, H., Kasper-Giebl, A., Loflund, M., Giebl, H., Hitzemberger, R., Zibuschka, F., and Puxbaum, H.: The contribution of bacteria and fungal spores to the organic carbon content of cloud water, precipitation and aerosols, Atmos. Res., 64, 109–119, 2002.

Burrows, S. M., Elbert, W., Lawrence, M. G., and Pöschl, U.: Bacteria in the global atmosphere – Part I: Review and synthesis of literature data for different ecosystems, Atmos. Chem. Phys., 9, 9263–9280, 2009.

Carlin, J. T., Reeves, H. D., & Ryzhkov, A. V.: Polarimetric Observations and Simulations of Sublimating Snow: Implications for Nowcasting, Journal of Applied Meteorology and Climatology, 60(8), 1035-1054, 2021.

Chen, Q., Yin, Y., Jiang, H., Chu, Z., Xue, L., Shi, R., et al. : The roles of mineral dust as cloud condensation nuclei and ice nuclei during the evolution of a hail storm. *Journal of Geophysical Research: Atmospheres*, 2019; 124: 14262– 14284, 2019.

Chin, M., Rood, R. B., Lin, S. J., Müller, J. F., and Thompson, A. M.: Atmospheric sulfur cycle simulated in the global model GOCART: Model description and global properties. *Journal of Geophysical Research Atmospheres*, 105, 24671–24687, <https://doi.org/10.1029/2000JD900384>, 2000.

Crawford, I., Bower, K. N., Choularton, T. W., Dearden, C., Crosier, J., Westbrook, C., Capes, G., Coe, H., Connolly, P. J., Dorsey, J. R., Gallagher, M. W., Williams, P., Trembath, J., Cui, Z., and Blyth, A.: Ice formation and development in aged, wintertime cumulus over the UK: observations and modelling, Atmos. Chem. Phys., 12, 4963–4985, <https://doi.org/10.5194/acp-12-4963-2012>, 2012.

Cui, Z., and Carslaw, K. S.: Enhanced vertical transport efficiency of aerosol in convective clouds due to increases in tropospheric aerosol abundance, J. Geophys. Res., 111, D15212, doi:10.1029/2005JD006781, 2006.

Deshmukh, A., Phillips, V. J. T. P., Bansemmer, A., Patade, S., and Waman, D.: New Empirical Formulation for the Sublimational Breakup of Graupel and Dendritic Snow, DOI: <https://doi.org/10.1175/JAS-D-20-0275.1>, 2021.

Deleted: ¶

Deleted: ¶

Deleted: . 1993

Deleted: (

Deleted: 2017).

Deleted: .

Deleted: . 2009

Deleted: ¶

Deleted: . 2021

Deleted: .

Deleted: (2019).

Deleted: .

Moved down [7]: R. B.

Moved down [8]: S. J.

Moved down [9]: J. F.

Moved down [10]: A. M.

Moved (insertion) [7]

Moved (insertion) [8]

Moved (insertion) [9]

Moved (insertion) [10]

Deleted: . 2000

Deleted: .

Moved down [11]: K. S.

Moved (insertion) [11]

Deleted: 2006

Deleted: Vaughan T. J.

Deleted: Aaron

Deleted: Sachin

Deleted: Deepak

Deleted: . 2021

Després, V. R., and Coauthors: Primary biological aerosol particles in the atmosphere: A review. *Tellus, Series B: Chemical and Physical Meteorology*, **64**, <https://doi.org/10.3402/tellusb.v64i0.15598>, 2012.

DeMott P. J., Prenni, A. J., Liu, X., Kreidenweis, S. M., Petters, M. D., Twohy, C.H., et al. Predicting global atmospheric ice nuclei distributions and their impacts on climate Proc. Natl. Acad. Sci. U. S. A., 107, pp. 11217-11222, 2010.

DeMott, P. J. and Prenni, A. J.: New Directions: Need for defining the numbers and sources of biological aerosols acting as ice nuclei, *Atmos. Environ.*, 44, 1944–1945, 2010.

Després, V.R., Huffman, J. A., Burrows, S. M., Hoose, C., Safatov, A. S., Buryak, G., Fröhlich-Nowoisky, J., Elbert, W., Andreae, M. O., Pöschl, U.: Primary biological aerosol particles in the atmosphere: a review. *Tellus B Chem. Phy. Meteorol.* 64 (1), 15598, 2012.

Dong, X., Mace, and G. G.: Arctic stratus cloud properties and radiative forcing derived from ground-based data collected at Barrow, Alaska. *J. Climate*, **16**, 445–461, doi:10.1175/1520-0442(2003)016<0445:ASCPAR>2.0.CO;2, 2003.

Han, B., Fan, J., Varble, A., Morrison, H., Williams, C. R., Chen, B., et al.: Cloud-resolving model intercomparison of an MC3E squall line case: Part II. Stratiform precipitation properties. *Journal of Geophysical Research: Atmospheres*, 124, 1090– 1117, 2019.

Fan, J., Liu, Y-C, Xu, K M., North, K., Collis, S., Dong, X., Zhang, G.J., Chen, Q., Kollias, P., and Ghan, S.J.: Improving representation of convective transport for scale-aware parameterization: 1. Convection and cloud properties simulated with spectral bin and bulk microphysics. *J. Geophys. Res. Atmos.*, 120, 3485– 3509. doi: 10.1002/2014JD022142, 2015.

Fan J., Comstock J.M., Ovchinnikov M.: The cloud condensation nuclei and ice nuclei effects on tropical anvil characteristics and water vapor of the tropical tropopause layer *Environ. Res. Lett.*, 5 Article 044005, 10.1088/1748-9326/5/4/044005, 2010.

Fan, J., Han, B., Varble, A., Morrison, H., North, K., Kollias, P., Chen, B., Dong, X., Giangrande, S., Khain, A., Lin, Y., Mansell, E., Milbrandt, J. A., Stenz, R., Thompson, G., Wang Y.: Cloud-resolving model intercomparison of an MC3E squall line case: Part I—Convective updrafts, *J. Geophys. Res. Atmos.*, 122, 9351– 9378, 2017.

Field, P. R., and Heymsfield A. J.: Importance of snow to global precipitation, *Geo-phys. Res. Lett.*, 42, 9512–9520, doi:10.1002/2015GL065497, 2015.

Deleted: s, 2012

Deleted: .

Moved down [12]: A.J.

Moved down [13]: M.D.

Moved (insertion) [12]

Moved (insertion) [13]

Deleted: X. Liu, X., S.M.

Deleted: C.H. Twohy, C.H., et al. Predicting global

Deleted: , 2012. Primary

Moved down [14]: and G. G.

Moved (insertion) [14]

Deleted: , 2003: Arctic stratus cloud properties and

Deleted: (2019). Cloud-resolving model intercomparison

Deleted: , Liu, Y-C, Xu, K-..., North, K., Collis,

Deleted: J.M. ...omstock J.M., M. ...vchinnikov M.,

Deleted: Bin Han, B., Adam ...arble, A., Hugh ...orriso

Moved down [15]: A. J.

Moved (insertion) [15]

Deleted: . (2015): ...mportance of snow to global

Field, P. R., Heymsfield, A. J., & Bansemer, A.: Shattering and Particle Interarrival Times Measured by Optical Array Probes in Ice Clouds, *Journal of Atmospheric and Oceanic Technology*, 23(10), 1357-1371, 2006.

Fridlind, A. M., and Coauthors: Derivation of aerosol profiles for MC3E convection studies and use in simulations of the 20 May squall line case. *Atmospheric Chemistry and Physics*, 17, 5947–5972, <https://doi.org/10.5194/acp-17-5947-2017>, 2017.

Fröhlich-Nowoisky, J., Kampf, C. J., Weber, B., Huffman, J.A., Pöhlker, C., Andreae, M. O., Lang-Yona, N., Burrows, S.M., Gunthe, S.S., Elbert, W., Su, H., Hoor, P., Thines, E., Hoffmann, T., Després, V.R., Pöschl, U.: Bioaerosols in the Earth system: climate, health, and ecosystem interactions. *Atmos. Res.* 182, 346–376, 2016.

Garcia, E., Hill, T. C. J., Prenni, A. J., DeMott, P. J., Franc, G. D., and Kreidenweis, S. M.: Biogenic ice nuclei in boundary layer air over two US high plains agricultural regions. *Journal of Geophysical Research Atmospheres*, 117, 1–12, <https://doi.org/10.1029/2012JD018343>, 2012.

Giangrande, S. E., Collis, S., Theisen, A. K., and Tokay, A.: Precipitation estimation from the ARM distributed radar network during the MC3E campaign. *Journal of Applied Meteorology and Climatology*, 53, 2130–2147, <https://doi.org/10.1175/JAMC-D-13-0321.1>, 2014.

Grützun, V., Knoth, O., and Simmel, M.: Simulation of the influence of aerosol particle characteristics on clouds and precipitation with LM-SPECS: Model description and first results. *Atmospheric Research*, 90, 233–242, <https://doi.org/10.1016/j.atmosres.2008.03.002>, 2008.

Hallett, J., and Mossop, S. C.: Production of secondary ice particles during the riming process. *Nature*, 249, 26–28, <https://doi.org/10.1038/249026a0>, 1974.

Heymsfield, A. J., Schmitt, C., Chen, C., Bansemer, A., Gettelman, A., Field, P. R., & Liu, C.: Contributions of the Liquid and Ice Phases to Global Surface Precipitation: Observations and Global Climate Modeling, *Journal of the Atmospheric Sciences*, 77(8), 2629–2648, 2020.

Hoose, C., and Möhler, O.: Heterogeneous ice nucleation on atmospheric aerosols: A review of results from laboratory experiments. *Atmospheric Chemistry and Physics*, 12, 9817–9854, <https://doi.org/10.5194/acp-12-9817-2012>, 2012.

Hoose, C., Kristjánsson, J. E., and Burrows, S. M.: How important is biological ice nucleation in clouds on a global scale? *Environmental Research Letters*, 5, <https://doi.org/10.1088/1748-9326/5/2/024009>, 2010.

Hoose, C., Kristjánsson, J. E., Chen, J. P., and Hazra, A.: A Classical-Theory-Based Parameterization of Heterogeneous Ice Nucleation by Mineral Dust, Soot, and Biological Particles in a Global Climate Model, *J. Atmos. Sci.*, 67, 2483–2503, <https://doi.org/10.1175/2010jas3425.1>, 2010b.

Huang, S., Wei, H., Chen, J., Wu, Z., Zhang, D., Fu, P.: Overview of biological ice nucleating particles in the atmosphere, *Environment International*, Volume 146, 106197, 2021.

- Deleted: (2006). Shattering and Particle Interarrival Times
- Deleted: , 2017
- Deleted: .
- Deleted: , 2016. Bioaerosols in the Earth
- Moved down [32]: T. C. J.
- Moved down [33]: A. J.
- Moved down [34]: P. J.
- Moved down [35]: G. D.
- Moved down [36]: S. M.
- Moved (insertion) [32]
- Moved (insertion) [33]
- Moved (insertion) [34]
- Moved (insertion) [35]
- Moved (insertion) [36]
- Deleted: , 2012
- Deleted: .
- Moved down [16]: A. K.
- Moved (insertion) [16]
- Deleted: S.
- Deleted: A. Tokay, A., 2014
- Deleted: .
- Deleted: O. Knoth, O., and M. ...immel, M., 2008
- Deleted: .
- Moved down [17]: S. C.
- Moved (insertion) [17]
- Deleted: , 1974
- Deleted: .
- Deleted: (2020).
- Deleted: O. Möhler, O., 2012
- Deleted: .
- Moved down [19]: J. E.
- Moved down [18]: S. M.
- Moved (insertion) [19]
- Moved (insertion) [18]
- Deleted: , 2010
- Deleted: .
- Deleted: -
- Deleted: u, Jie ...hen, J., Zhijun...Wu, Z., Daizhou

Huffman, J. A., and Coauthors: High concentrations of biological aerosol particles and ice nuclei during and after rain. *Atmospheric Chemistry and Physics*, **13**, 6151–6164, <https://doi.org/10.5194/acp-13-6151-2013>, 2013.

Hummel, M., Hoose, C., Pummer, B., Schaupp, C., Fröhlich-Nowoisky, J., and Möhler, O.: Simulating the influence of primary biological aerosol particles on clouds by heterogeneous ice nucleation. *Atmospheric Chemistry and Physics*, **18**, 15437–15450, <https://doi.org/10.5194/acp-18-15437-2018>, 2018.

Jensen, M. P., and Coauthors: The midlatitude continental convective clouds experiment (MC3E). *Bulletin of the American Meteorological Society*, **97**, 1667–1686, <https://doi.org/10.1175/BAMS-D-14-00228.1>, 2016.

Jaenicke, R.: Abundance of cellular material and proteins in the atmospheric. *Science* **308**, 73, 2005.

Kanji, Z. A., Ladino, L. A., Wex, H., Boose, Y., Burkert-Kohn, M., Cziczo, D. J., & Krämer, M.: Overview of Ice Nucleating Particles, *Meteorological Monographs*, **58**, 1.1-1.33, 2017.

Korolev, A. V., Kuznetsov, S. V., Makarov, Y. E., & Novikov, V. S.: Evaluation of Measurements of Particle Size and Sample Area from Optical Array Probes, *Journal of Atmospheric and Oceanic Technology*, **8**(4), 514–522, 1991.

Korolev, A., McFarquhar, G., Field, P. R., Franklin, C., Lawson, P., Wang, Z., Williams, E., Abel, S. J., Axisa, D., Borrmann, S., Crosier, J., Fugal, J., Krämer, M., Lohmann, U., Schlenczek, O., Schnaiter, M., & Wendisch, M.: Mixed-Phase Clouds: Progress and Challenges, *Meteorological Monographs*, **58**, 5.1-5.50, 2017.

Korolev, A. and Leisner, T.: Review of experimental studies of secondary ice production, *Atmos. Chem. Phys.*, **20**, 11767–11797, <https://doi.org/10.5194/acp-20-11767-2020>, 2020.

Korolev, A., Heckman, I., Wolde, M., Ackerman, A. S., Fridlind, A. M., Ladino, L. A., Lawson, R. P., Milbrandt, J., and Williams, E.: A new look at the environmental conditions favorable to secondary ice production, *Atmos. Chem. Phys.*, **20**, 1391–1429, <https://doi.org/10.5194/acp-20-1391-2020>, 2020.

Kumjian, M. R. and Lombardo, K. A.: Insights into the evolving microphysical and kinematic structure of northeastern U.S. winter storms from dual-polarization Doppler radar. *Mon. Wea. Rev.*, **145**, 1033–1061, <https://doi.org/10.1175/MWR-D-15-0451.1>, 2017.

Knopf, D. A., Alpert, P. A., Wang, B., Aller, J. Y.: Stimulation of ice nucleation by marine diatoms. *Nat. Geosci.* **4**, 88–90. <https://doi.org/10.1038/ngeo1037>, 2011.

Lawson, R. P., Woods, S. and Morrison, H.: The microphysics of ice and precipitation development in tropical cumulus clouds, *J. Atmos. Sci.*, **72**(6), 2429–2445, 1196 doi:10.1175/JAS-D-14-0274.1, 2015.

Levin, Z., Yankofsky, S., Pardes, D. and Magal, N.: *J. Clim. Appl. Meteorol.* **26** 1188–97, 1987.

Deleted: , 2013

Deleted: .

Deleted: C.

Deleted: B.

Deleted: C.

Deleted: J.

Deleted: O.

Deleted: , 2018

Deleted: .

Deleted: , 2016

Deleted: .

Deleted: , 2005.

Deleted: .

Deleted: (2017).

Deleted: .

Deleted: . (1991).

Deleted: .

Deleted: Korolev, A. V., Emery, E. F., Strapp, J. W., Cober, S. G., Isaac, G. A., Wasey, M., & Marcotte, D. (2011). Small Ice Particles in Tropospheric Clouds: Fact or Artifact? Airborne Icing Instrumentation Evaluation Experiment, *Bulletin of the American Meteorological Society*, **92**(8), 967–973

Deleted: (2017).

Moved down [20]: K. A.

Moved (insertion) [20]

Deleted: ., 2017

Deleted: .

Deleted: , 2011.

Deleted: ., 2015

Deleted: , 1987,

1757 Matus, A. V. and L'Ecuyer, T. S.: The role of cloud phase in Earth's radiation budget, *J.*
1758 *Geophys. Res. Atmos.*, 122, 2559– 2578, doi:10.1002/2016JD025951, 2017.

1759 Malm, W. C., Sisler, J. F., Huffman, D., Eldred, R. A., and Cahill, T. A.: Spatial and seasonal
1760 trends in particle concentration and optical extinction in the United States, *J. Geophys.*
1761 *Res.*, 99, 1347-1370, 1994.

1762 Matthias-Maser, S., Bogs, B., Jaenicke, R.: The size distribution of primary biological
1763 aerosol particles in cloud water on the mountain Kleiner Feldberg/Taunus (FRG),
1764 *Atmospheric Research*, Volume 54, Issue 1, Pages 1-13, 2000.

1765 Mattias-Maser, S., Brinkmann, J., Schneider, W.: The size distribution of marine atmospheric
1766 aerosol with regard to primary biological aerosol particles over the South Atlantic
1767 Ocean. *Atmospheric Environment* 33, 3569–3575, 1999.

1768 Mattias-Maser, S., Jaenicke, R.: The size distribution of primary biological aerosol particles
1769 with radii > 0.2 mm in an urban/rural influenced region. *Atmospheric Research* 39, 279–
1770 286, 1995.

1771 Mülmenstädt, J., Sourdeval, O., Delanoë, J., and Quaas, J.: Frequency of occurrence of rain
1772 from liquid-, mixed-, and ice-phase clouds derived from A-Train satellite retrievals,
1773 *Geophys. Res. Lett.*, 42, 6502– 6509, 2015.

1778 Möhler, O., and Coauthors: *Heterogeneous ice nucleation activity of bacteria: new*
1779 *laboratory experiments at simulated cloud conditions*. 1425–1435 pp.
1780 www.biogeosciences.net/5/1425/2008/, 2008.

1781 Moisseev, D. N., Lautaportti, S., Tyynela, J., and Lim, S. (2015), Dual-polarization radar
1782 signatures in snowstorms: Role of snowflake aggregation, *J. Geophys. Res.*
1783 *Atmos.*, 120, 12644– 12655, doi:10.1002/2015JD023884.

1784 Morris, C. E., Conen, F., Huffman, A. J., Phillips, V. J. T. P., Pöschl, U., and Sands, D. C.:
1785 Bioprecipitation: A feedback cycle linking Earth history, ecosystem dynamics and land
1786 use through biological ice nucleators in the atmosphere. *Global Change Biology*, 20,
1787 341–351, <https://doi.org/10.1111/gcb.12447>, 2014.

1788 Murray, B. J., O'Sullivan, D., Atkinson, J. D., and Webb, M. E.: Ice nucleation by particles
1789 immersed in supercooled cloud droplets. *Chem. Soc. Rev.*, 41, 6519–6554,
1790 <https://doi.org/10.1039/c2cs35200a>, 2012.

1791 Patade, S., Phillips, V. T. J., Amato, P., Bingemer, H. G., Burrows, S. M., DeMott, P. J.,
1792 Goncalves, F. L. T., Knopf, D. A., Morris, C. E., Alwmark, C., Artaxo, P., Pöhlker, C.,
1793 Schrod, J., & Weber, B.: Empirical Formulation for Multiple Groups of Primary
1794 Biological Ice Nucleating Particles from Field Observations over Amazonia, *Journal of*
1795 *the Atmospheric Sciences*, 78(7), 2195-2220, 2021.

1796 Phillips, V. T. J., Donner, L. J., and Garner, S.: Nucleation processes in deep convection
1797 simulated by a cloud-system resolving model with double-moment bulk microphysics, *J.*
1798 *Atmos. Sci.*, 64, 738– 761, 2007.

Deleted: . (2017),

Deleted: .

Moved down [21]: J. F.

Moved down [22]: R. A.

Moved down [23]: T. A.

Moved (insertion) [21]

Moved (insertion) [22]

Moved (insertion) [23]

Deleted: D.

Deleted: (1994).

Deleted: .

Deleted: Berit

Deleted: Ruprecht

Deleted: ,

Deleted: 2000,

Deleted: , 1999.

Deleted: .

Deleted: , 1995.

Deleted: (2015),

Deleted: , 2008

Deleted: .

Moved down [31]: D. C.

Moved (insertion) [31]

Deleted: F.

Deleted: J. Alex

Deleted: V.

Deleted: U.

Deleted: 2014

Deleted: .

Moved down [29]: J. D.

Moved down [30]: M. E.

Moved (insertion) [29]

Moved (insertion) [30]

Deleted: D.

Deleted: 2012

Deleted: (2021).

Deleted: .

1830 Phillips, V. T. J., DeMott, P. J., & Andronache, C.: An Empirical Parameterization of
 1831 Heterogeneous Ice Nucleation for Multiple Chemical Species of Aerosol, *Journal of the*
 1832 *Atmospheric Sciences*, 65(9), 2757-2783, 2008.

1833 Phillips, V. T. J., and Coauthors: Potential impacts from biological aerosols on ensembles of
 1834 continental clouds simulated numerically. *Biogeosciences*, 6, 987–1014,
 1835 <https://doi.org/10.5194/bg-6-987-2009>, 2009

1836 Phillips, V. T. J., Yano, J., Formenton, M., Ilotoviz, E., Kanawade, V., Kudzotsa, I., Sun, J.,
 1837 Bansemer, A., Detwiler, A. G., Khain, A., & Tessoroff, S. A.: Ice Multiplication by
 1838 Breakup in Ice–Ice Collisions. Part II: Numerical Simulations, *Journal of the*
 1839 *Atmospheric Sciences*, 74(9), 2789-2811, 2017b.

1840 Phillips, V. T. J., Formenton, M., Kanawade, V. P., Karlsson, L. R., Patade, S., Sun, J.,
 1841 Barthe, C., Pinty, J., Detwiler, A. G., Lyu, W., & Tessoroff, S. A.: Multiple
 1842 Environmental Influences on the Lightning of Cold-Based Continental Cumulonimbus
 1843 Clouds. Part I: Description and Validation of Model, *Journal of the Atmospheric*
 1844 *Sciences*, 77(12), 3999-4024, 2020.

1845 Phillips, V. T. J., Yano, J. I., and Khain, A.: Ice multiplication by breakup in ice-ice
 1846 collisions. Part I: Theoretical formulation. *Journal of the Atmospheric Sciences*, 74,
 1847 1705–1719, <https://doi.org/10.1175/JAS-D-16-0224.1>, 2017a.

1848 Phillips, V. T. J., Demott, P. J., Andronache, C., Pratt, K. A., Prather, K. A., Subramanian,
 1849 R., and Twohy, C.: Improvements to an empirical parameterization of heterogeneous ice
 1850 nucleation and its comparison with observations. *Journal of the Atmospheric Sciences*,
 1851 70, 378–409, <https://doi.org/10.1175/JAS-D-12-080.1>, 2013.

1852 Phillips, V. T. J., Patade, S.: Multiple Environmental Influences on the Lightning of Cold-
 1853 based Continental Convection. Part II: Sensitivity Tests for its Charge Structure and
 1854 Land-Ocean Contrast. *Journal of the Atmospheric Sciences*,
 1855 <https://doi.org/10.1175/JAS-D-20-0234.1>, 2021.

1856 Phillips, V. T. J., Patade, S., Gutierrez, J., and Bansemer, A.: Secondary ice production by
 1857 fragmentation of freezing drops: Formulation and theory. *Journal of the Atmospheric*
 1858 *Sciences*, 75, 3031–3070, <https://doi.org/10.1175/JAS-D-17-0190.1>, 2018.

1859 Prenni, A. J., and Coauthors: The impact of rain on ice nuclei populations at a forested site in
 1860 Colorado. *Geophysical Research Letters*, 40, 227–231,
 1861 <https://doi.org/10.1029/2012GL053953>, 2013.

1862 Pörtner, H. O., et al.: Summary for policymakers. In: Climate change 2022: Impact,
 1863 adaptation, and vulnerability: Summary for policy makers: Working group II
 1864 Contribution to the sixth assessment report of the Intergovernmental Panel on Climate
 1865 Change, 2022.

1866 Ryzhkov, A., Pinsky, M., Pokrovsky, A., & Khain, A.: Polarimetric Radar Observation
 1867 Operator for a Cloud Model with Spectral Microphysics, *Journal of Applied*
 1868 *Meteorology and Climatology*, 50(4), 873-894, 2011.

1869 Sahyoun, M., Wex, H., Gosewinkel, U., Šantl-Temkiv, T., Nielsen, N. W., Finster, K.,
 1870 Sørensen, J. H., Stratmann, F., and Korsholm, U. S.: On the usage of classical nucleation

Deleted: (2008).

Deleted: .

Deleted: , 2009

Deleted: . (2017).

Deleted: .

Deleted: (2020).

Moved down [28]: J. I.

Moved (insertion) [28]

Deleted: A.

Deleted: 2017c

Deleted: .

Moved down [25]: P. J.

Moved down [26]: K. A.

Moved down [27]: K. A.

Moved (insertion) [25]

Moved (insertion) [26]

Deleted: C.

Moved (insertion) [27]

Deleted: R.

Deleted: C.

Deleted: 2013

Deleted: .

Deleted: S.

Deleted: , 2021

Deleted: S.

Deleted: J.

Deleted: A.

Deleted: , 2018

Deleted: .

Deleted: , 2013

Deleted: .

Deleted: Hans

Deleted: , 2022

Deleted: .

Deleted: (2011).

theory in quantification of the impact of bacterial INP on weather and climate, *Atmos. Environ.*, 139, 230–240, <https://doi.org/10.1016/j.atmosenv.2016.05.034>, 2016.

Sesartic, A., Lohmann, U., and Storelvmo, T.: Bacteria in the ECHAM5-HAM global climate model. *Atmospheric Chemistry and Physics*, **12**, 8645–8661, <https://doi.org/10.5194/acp-12-8645-2012>, 2012.

Sesartic, A., Lohmann, U., and Storelvmo, T.: Modelling the impact of fungal spore ice nuclei on clouds and precipitation. *Environmental Research Letters*, **8**, <https://doi.org/10.1088/1748-9326/8/1/014029>, 2013.

Sinclair, V. A., Moisseev, D., and von Lerber, A. (2016), How dual-polarization radar observations can be used to verify model representation of secondary ice, *J. Geophys. Res. Atmos.*, 121, 10,954– 10,970, doi:10.1002/2016JD025381.

Sotiropoulou, G., Ickes, L., Nenes, A. and Ekman, A.: Ice multiplication from ice–ice collisions in the high Arctic; sensitivity to ice habit, rimed fraction, ice type and uncertainties in the numerical description of the process, *Atmos. Chem. Phys.*, 21, 9741–9760, 1313 doi:10.5194/acp-21-9741-2021, 2021b

Sotiropoulou, G., Vignon, E., Young, G., Morrison, H., O’Shea, S. J., Lachlan-Cope, T., Berne, A. and Nenes, A.: Secondary ice production in summer clouds over the Antarctic coast: 1308 An underappreciated process in atmospheric models, *Atmos. Chem. Phys.*, 21(2), 755– 1309 771, doi:10.5194/acp-21-755-2021, 2021a.

Spracklen, D. V., and Heald, C. L.: The contribution of fungal spores and bacteria to regional and global aerosol number and ice nucleation immersion freezing rates. *Atmospheric Chemistry and Physics*, **14**, 9051–9059, <https://doi.org/10.5194/acp-14-9051-2014>, 2014

Szyrmer, W., Zawadzki, I.: Biogenic and anthropogenic sources of ice-forming nuclei: A review. *Bull. Am. Meteorol. Soc.* 78, 209–228, 1997.

Tsushima, Y., Emori, S., Ogura, T., et al.: Importance of the mixed-phase cloud distribution in the control climate for assessing the response of clouds to carbon dioxide increase: a multi-model study. *Clim Dyn* 27, 113–126, 2006.

Wilson, T., and Coauthors: A marine biogenic source of atmospheric ice-nucleating particles. *Nature*, 525, 234–238, <https://doi.org/10.1038/nature14986>, 2015.

Xie, S., Y. Zhang, S. E. Giangrande, M. P. Jensen, R. McCoy, and M. Zhang: Interactions between cumulus convection and its environment as revealed by the MC3E sounding array. *Journal of Geophysical Research*, **119**, 11,784–11,808, <https://doi.org/10.1002/2014JD022011>, 2014.

Zhao, X., & Liu, X.: Global importance of secondary ice production. *Geophysical Research Letters*, 48, e2021GL092581. <https://doi.org/10.1029/2021GL092581>, 2021.

Zuidema, P., E. R. Westwater, C. Fairall, and Hazen, D.: Ship-based liquid water path estimates in marine stratocumulus. *J. Geophys. Res.*, **110**, D20206, doi:10.1029/2005JD005833, 2005.

Deleted: U.

Deleted: T.

Deleted: , 2012

Deleted: .

Deleted: U.

Deleted: T.

Deleted: , 2013

Deleted: .

Deleted: 2021b

Deleted: 2021a

Moved down [24]: C. L.

Moved (insertion) [24]

Deleted: v

Deleted: , 2014

Deleted: .

Deleted: .

Deleted: 1997.

Deleted: .

Deleted: S.

Deleted: T.

Deleted: .

Deleted: , 2006

Deleted: (2006). <https://doi.org/10.1007/s00382-006-0127-7>, ...

Deleted: , 2015

Deleted: .

Deleted: , 2014

Deleted: .

Deleted: (2021).

Deleted: D.

Deleted: , 2005

Formatted: Indent: Left: 0 cm, Hanging: 0,85 cm, Line spacing: Multiple 1,07 li, Don't adjust space between Latin and Asian text, Don't adjust space between Asian text and numbers

Deleted: ¶

¶